

# Multi-model assessment of the deglacial climatic evolution at high southern latitudes

Takashi Obase<sup>1,2</sup>, Laurie Menviel<sup>3</sup>, Ayako Abe-Ouchi<sup>1</sup>, Tristan Vadsaria<sup>1,4\*</sup>, Ruza Ivanovic<sup>5</sup>, Brooke Snoll<sup>5</sup>, Sam Sherriff-Tadano<sup>5</sup>, Paul J. Valdes<sup>6</sup>, Lauren Gregoire<sup>5</sup>, Marie-Luise Kapsch<sup>7</sup>, Uwe Mikolajewicz<sup>7</sup>, Nathaëlle Bouttes<sup>8</sup>, Didier Roche<sup>8</sup>, Fanny Lhardy<sup>8\*\*</sup>, Chengfei He<sup>9</sup>, Bette Otto-Bliesner<sup>10</sup>, Zhengyu Liu<sup>11</sup>, Wing-Le Chan<sup>1</sup>

<sup>1</sup>Atmosphere and Ocean Research Institute, The University of Tokyo, Kashiwa, Japan

<sup>2</sup>Japan Agency for Marine-Earth Science and Technology, Yokohama, Japan

<sup>3</sup>Climate Change Research Center, The Australian Centre for Excellence in Antarctic Science, the University of New South Wales, Sydney, Australia,

<sup>4</sup>UiT The Arctic University of Norway, Tromsø, Norway

<sup>5</sup>School of Earth & Environment, University of Leeds, Woodhouse Lane, Leeds, UK

<sup>6</sup>School of Geographical Sciences, University of Bristol, University Road, Bristol, UK

<sup>7</sup>Max Planck Institute for Meteorology, Hamburg, Germany

<sup>8</sup>Laboratoire des Sciences du Climat et de l'Environnement/Institut Pierre-Simon Laplace, UMR CEA-CNRS-UVSQ, Université Paris-Saclay, Gif-sur-Yvette, France

<sup>9</sup>Woods Hole Oceanographic Institution, Woods Hole, MA, USA

<sup>10</sup>Climate and Global Dynamics Laboratory, National Center for Atmospheric Research, Boulder, USA

<sup>11</sup>Atmospheric Science Program, Department of Geography, Ohio State University, Columbus, USA

\*Now at Biogéosciences, UMR 6282 CNRS, Université Bourgogne Europe, 6 boulevard Gabriel, 21000 Dijon, France

\*\*Now at Laboratoire de Géologie de Lyon Terre - Planètes - Environnement, École Normale Supérieure de Lyon, 46, allée d'Italie, 69007 Lyon, France

*Correspondence to:* Takashi Obase ([tobase@jamstec.go.jp](mailto:tobase@jamstec.go.jp))

**Abstract.** The Quaternary climate is characterised by glacial-interglacial cycles, with the most recent transition from the last glacial maximum to the present interglacial (the last deglaciation) occurring between ~ 21 and 9 ka. While the deglacial warming at high southern latitudes is mostly in phase with atmospheric CO<sub>2</sub> concentrations, some proxy records indicate that the onset of the warming occurred before the CO<sub>2</sub> increase. In addition, high southern latitudes exhibit a cooling event in the middle of the deglaciation (15 - 13 ka) known as the ‘Antarctic Cold Reversal’. In this study, we analyse transient simulations of the last deglaciation performed with six different climate models as part of the 4th phase of the Paleoclimate Modelling Intercomparison Project (PMIP4) to understand the processes driving high southern latitude surface temperature changes. As the protocol of the last deglaciation sets the choice of

freshwater forcing as flexible, the freshwater forcing is different in each model, thus complicating the multi-model comparison. While proxy records from West Antarctica and the Pacific sector of the Southern Ocean suggest the presence of an early warming before 18 ka, only half the models show a significant warming at this time ( $\sim 1^{\circ}\text{C}$  or  $\sim 10\%$  of the total deglacial warming). All models simulate a major warming during Heinrich stadial 1 (18 - 15 ka) concurrent with the  $\text{CO}_2$  increase and with a weakening of the Atlantic Meridional Overturning Circulation (AMOC) in some models. However, the simulated Heinrich Stadial 1 warming over Antarctica is smaller than the one suggested from ice core data. During the Antarctic Cold Reversal, simulations with an abrupt AMOC strengthening exhibit a high southern latitude cooling of 1 to  $2^{\circ}\text{C}$ , in relative agreement with proxy records, while simulations with rapid North Atlantic meltwater input exhibit a warming. Using simple models to extract the relative AMOC contribution, we find that all climate models simulate a high southern latitude cooling in response to an AMOC increase with a response timescale of several hundred years, suggesting the choice of the North Atlantic meltwater forcing substantially affects high southern latitudes temperature changes. Thus, further work needs to be carried out to reconcile the deglacial AMOC evolution with the Northern Hemisphere ice sheet disintegration and associated meltwater input. Finally, all simulations exhibit only minimal changes in Southern Hemisphere westerlies and Southern Ocean meridional circulation during the last deglaciation. Improved understanding of the processes impacting Southern Hemisphere atmospheric and oceanic circulation changes accounting for deglacial atmospheric  $\text{CO}_2$  increase are needed.

## **1. Introduction**

The recent Quaternary climate is characterised by glacial-interglacial cycles with a periodicity of about 100,000 years (Lisiecki and Raymo, 2005; Jouzel et al., 2007). These glacial-interglacial cycles are driven by insolation changes as the external forcing and by internal feedbacks, including changes in atmospheric greenhouse gas concentrations and continental ice sheets (Abe-Ouchi et al., 2013). During the Last Glacial Maximum (LGM,  $\sim 21$  ka; ka indicates 1000 years before present), the continental ice sheets covered a significant area of the high northern latitudes (Tarasov et al., 2012; Peltier et al., 2015), thus leading to a sea level fall of  $\sim 130$  meters compared to pre-industrial (Lambeck et al., 2014). The

61 atmospheric CO<sub>2</sub> concentration was also ~100 ppm lower than pre-industrial (Petit et al., 1999; Bereiter  
62 et al., 2015). These climatic boundary conditions contributed to a colder climate during the LGM, with  
63 global mean surface air temperature anomalies estimated to be 4 to 7 °C lower than present-day (Annan  
64 et al., 2022; Liu et al., 2023). As the last deglaciation (transition from the LGM to the early Holocene ~11  
65 ka) represents one of the largest, most recent and well-documented natural warmings of the last million  
66 years, an understanding of the processes and feedbacks during this time period can offer insight into our  
67 own modern changing world. Here, we focus on the high southern latitudes, where deglacial warming  
68 began before the Northern Hemisphere (NH) counterparts (Shakun et al., 2012); it has been suggested  
69 that processes here played a major role in driving the increase in atmospheric CO<sub>2</sub> concentration.  
70 Although the timing of the onset of the deglacial warming at high southern latitudes is poorly constrained,  
71 a compilation of Antarctic ice core records from East Antarctica suggests that the deglacial Antarctic  
72 warming started at ~18 ka, in phase with the rise in atmospheric CO<sub>2</sub> concentration (Parrenin et al., 2013).  
73 On the other hand, a record from the West Antarctic Ice Sheet Divide ice core suggests that the warming  
74 started ~20 ka (Shakun et al., 2012; WAIS project members, 2013). Moreover, an early onset of the  
75 deglacial warming (~21 ka) at high and mid-southern latitudes has also been inferred from Sea Surface  
76 Temperature (SST) and sea ice records from the Pacific sector of the Southern Ocean (Moy et al., 2019;  
77 Sikes et al., 2019; Moros et al., 2021; Crosta et al., 2022; Sadatzki et al., 2023).

78         Millennial-scale climate events are superimposed on the more gradual deglacial warming trend.  
79 At the beginning of the deglaciation, during Heinrich stadial 1 (~18 to 14.7 ka, following Ivanovic et al.,  
80 2016), Greenland and the North Atlantic region remained cold (Buizert et al., 2014, Martrat et al., 2007),  
81 while significant warming occurred at high southern latitudes (WAIS project members, 2010). This period  
82 was associated with a weakening of the Atlantic Meridional Ocean Circulation (AMOC), evidenced by  
83 Pa/Th in marine sediments (McManus et al., 2004; Ng et al., 2018). During the subsequent Bølling-  
84 Allerød period (~14.7 to 12.8 ka), Greenland surface air temperatures rose by more than 10°C in just a  
85 few decades (Stephensen et al., 2008; Buizert et al., 2014), and the AMOC strengthened significantly  
86 (Severinghaus & Brook, 1999; McManus et al., 2004; Roberts et al., 2010; Ng et al., 2018). A cooling  
87 event at high southern latitudes, known as the Antarctic Cold Reversal, was identified between ~15 and  
88 13 ka (Jouzel et al. 2007; Pedro et al., 2016), concurrent with the Bølling-Allerød. The Younger-Dryas

(12.8 to 11.7 ka) followed the Bølling-Allerød, and was characterised by a drastic cooling in Greenland and the North Atlantic. While the processes leading to the Younger Dryas are still debated (Renssen et al., 2015), it has been suggested that the Younger Dryas could be attributed to a weakening of the AMOC (McManus et al., 2004), caused by a rerouting of freshwater into the Arctic that was then transported toward the deep-water formation sites of the subpolar North Atlantic by coastal boundary currents (Condon and Winsor, 2012; Kapsch et al., 2022). Climate model simulations with marine proxy constraints support the variations in the AMOC during the last deglaciation (Pöppelmeier et al., 2023).

An AMOC weakening causes a warming in the South Atlantic as the meridional oceanic heat transport to the North Atlantic is weakened (Stocker & Johnsen, 2003; Stouffer et al., 2006). This warming can then be propagated to the Southern Ocean and Antarctica (Pedro et al., 2018). The contrasting temperature changes between Greenland and the southern high latitudes can also be found during abrupt events of the last glacial period known as Dansgaard–Oeschger cycles (Dansgaard 1993; NGRIP project members, 2004; WAIS Divide project members, 2015), leading to the notion of a bipolar seesaw (Stocker and Johnsen 2003; Capron et al., 2010). Alongside these events, the atmospheric CO<sub>2</sub> increase throughout the deglaciation occurred in steps, suggesting a link with millennial-scale climate events (Marcott et al., 2014) and changes in Southern Ocean circulation contributing to degassing of oceanic carbon (Anderson et al., 2009, Menviel et al., 2018).

Transient climate simulations provide a suitable framework for assessing the processes leading to deglacial climate changes. Early transient simulations that were conducted with transient orbital forcing, greenhouse gases and ice sheets suggested that an increase in austral spring insolation in the southern high latitudes was responsible for the onset of warming (Timmermann et al., 2009), and that deglacial warming of the Southern Ocean appeared as early as ~20 to 18 ka in association with sea ice retreat (Roche et al., 2011). Transient simulations that also included freshwater input into the North Atlantic highlighted the AMOC impact on climate change (Liu et al., 2009; He et al., 2011). Menviel et al. (2011) further showed that the Antarctic Cold Reversal could be a response to the strong AMOC increase at the end of Heinrich Stadial 1, but that its length and amplitude could have been enhanced by meltwater input from the Antarctic ice sheet. These simulations were designed to simulate AMOC changes in agreement with estimates from proxy records, and therefore the magnitude, location, and timing of the implemented

meltwater fluxes were idealised. In contrast, experiments forced with meltwater fluxes consistent with ice sheet reconstructions based on sea-level constraints often simulate millennial-scale AMOC changes in disagreement with accepted interpretations of climate and ocean records (Snoll et al., 2024). Some experiments simulate an AMOC weakening at the time of the Bølling-Allerød because of significant mass loss of Northern Hemisphere ice sheets (Bethke et al., 2012; Ivanovic et al., 2018a; Kapsch et al., 2022; Bouttes et al., 2023) or do not simulate any abrupt climate events (Gregoire et al., 2012). With an idealised scenario that follows the evolution of Northern Hemisphere ice sheets more closely (except for the 14 ka meltwater pulse), the MIROC climate model shows that it is possible to simulate an abrupt AMOC strengthening with the presence of continuous freshwater in the North Atlantic because of gradual warming (Obase and Abe-Ouchi, 2019). These studies indicate that different models have different sensitivities in terms of the AMOC response to forcing and, therefore, it is useful to analyse multi-model results for a robust understanding of the climatic processes.

To facilitate further examination of the mechanisms driving deglacial climate change, a protocol for carrying out transient simulations of the last deglaciation was proposed as part of the fourth phase of the Paleoclimate Modeling Intercomparison Project (PMIP4) (Ivanovic et al., 2016). The PMIP4 last deglaciation model protocol summarised the climate forcings needed (ice core based atmospheric greenhouse gases and reconstructed ice sheets) for climate model experiments. The protocol is designed to be flexible in that the use of some boundary conditions is determined by each modelling group, which allows an exploration of different climate scenarios. The first PMIP multi-model study of the last deglaciation, focusing on the northern hemispheric climate during Heinrich Stadial 1, found that different freshwater approaches (*melt-uniform, melt-routed, trace-like, bespoke*; Snoll et al., 2024) have a dominant impact on North Atlantic climate variability. The multi-model assessment of the last deglaciation performed here provides an opportunity to investigate the processes impacting southern high latitude climate and to evaluate model sensitivity to the forcings.

Some boundary conditions for climate models, including greenhouse gases and Antarctic ice sheet (prescribed in PMIP4 protocol), result from climate change at high southern latitudes. Proxy records (Sigman et al., 2010, Skinner et al., 2010, Martinez-Garcia et al., 2011) and modelling studies (Bouttes et al., 2012, Menviel et al., 2016, Menviel et al., 2018, Gottschalk et al., 2019) indicate that physical and

biogeochemical changes in the Southern Ocean may have significantly contributed to ocean carbon uptake during the last glacial period and to the atmospheric CO<sub>2</sub> increase during Heinrich Stadial 1. Subsurface warming on the Antarctic shelf contributes to the mass loss of Antarctic ice sheets through enhanced melting of ice shelves, and retreat of grounding lines (Golledge et al., 2014; Lowry et al., 2019). In addition, climate conditions at high southern latitudes can impact the formation of Antarctic Bottom Water and the shoaling of AMOC (Sherriff-Tadano et al., 2023). Hence investigating the deglacial climate evolution at high southern latitudes may provide insight into critical climate system feedbacks.

Here, we analyse the deglacial climatic evolution (21–11 ka) at high southern latitudes as simulated in six PMIP4 transient experiments, and compare the results with paleo-proxy records. We focus on the magnitude and rate of changes in Antarctic surface air temperature (SAT) and Southern Ocean SST. As there is a substantial difference between the temporal evolution of AMOC strength in the simulations, we utilise statistical or simple models to separate the impact of changes in atmospheric CO<sub>2</sub> and AMOC on Southern Ocean SST. Finally, we analyse the evolution of Antarctic Bottom Water, Southern Ocean westerlies and subsurface ocean temperature in the to discuss critical climate system feedbacks occurring at high southern latitudes.

## 2 Methods

### 2-1 Climate models and experiments used in this study

We use the PMIP4 transient simulations of the last deglaciation performed with six atmosphere-ocean coupled climate models (Table 1), and analyse the time period from the LGM to the Early Holocene, 21–11 ka. Table 2 summarises the experimental design of each model describes the simulation (including LGM and pre-industrial climates). The LGM climate fields (initial condition of these experiments) have been evaluated by previous studies, particularly for global temperature changes (Kageyama et al. 2021), sea ice and SST changes in the Southern Ocean (Lhardy et al., 2021; Green et al. 2022), and SAT changes over the Antarctic ice sheet (Buizert et al. 2021). A part of the transient simulations utilized in this study have also been compared to proxy-reconstructions (Weitzel et al. 2024). Fig. S1 compares simulated sea-ice edges for the pre-industrial simulations from six models used in this study, showing that some models underestimate pre-industrial summer sea ice extent, but mostly to an acceptable level. The Equilibrium

173 Climate Sensitivity (ECS, defined by global mean SAT changes in response to doubling CO<sub>2</sub> from the  
174 pre-industrial) of each model ranges from 2.0 to 3.9 °C, and the global mean surface air temperature  
175 (SAT) anomaly for the LGM is 3.5 to 7.3 °C (Table 1).

176 While some of the modelling groups performed two or more sensitivity experiments with different  
177 model parameters or boundary conditions (e.g., different freshwater forcing ) scenarios or ice sheets), for  
178 this study we have selected one representative simulation from each climate model. Fig. 1 summarises  
179 the time evolution of the climate forcings, i.e. insolation, atmospheric greenhouse gases, and continental  
180 ice sheets used in the simulations. Both the PMIP4 recommended reconstructions (ICE-6G\_C VM5a,  
181 henceforth ‘ICE-6G\_C’; and ‘GLAC-1D’) have larger Antarctic ice sheet volume at the LGM, with a ~  
182 10 m sea-level equivalent volume change at the LGM, relative to present-day. Both suggest ~ 100 m of  
183 elevation reduction since the LGM at EPICA Dome C (EDC, 123°E, 75°S), while estimates of the  
184 elevation change at the West Antarctic Ice Sheet Divide (WDC, 112°W, 79.5°S) differs by 300 m between  
185 the two datasets (Fig. 1d).

186 Fig. 2a summarises the total amount of freshwater forcing in the Northern Hemisphere in six  
187 simulations. The freshwater forcing schemes can be classified into two groups: The first group  
188 characterises freshwater forcing that has been adjusted to reproduce large-scale AMOC variability  
189 (utilised in iTRACE, LOVECLIM and MIROC simulations), and the second group includes freshwater  
190 forcing consistent with the reconstructed ice volume changes (implemented in HadCM3, MPI-ESM,  
191 iLOVECLIM simulations) based on ICE-6G\_C or GLAC-1D (Fig. 2a, upper panel, red and black lines).  
192 Notably, during Heinrich Stadial 1, iTRACE and LOVECLIM have significant freshwater forcing (~ 0.2  
193 Sv), while other simulations (including MIROC) apply freshwater forcing of less than 0.1 Sv. In  
194 LOVECLIM and MIROC, the meltwater flux was uniformly applied to the North Atlantic, while other  
195 models use the location of ice sheet melting and associated runoff distribution to apply a spatially varying  
196 freshwater forcing (Table 2). ICE-6G\_C (HadCM3, MPI-ESM, iLOVECLIM) leads to a meltwater input  
197 of about 0.1 Sv to the Southern Ocean at 11.5–11 ka. iTRACE and LOVECLIM also applied a freshwater  
198 flux to the Southern Ocean to simulate the Antarctic Cold Reversal (iTRACE: up to 0.2Sv during 14.4–  
199 13.9 ka, LOVECLIM: fixed at 0.09Sv during 14.67–14.1 ka).

In section 3.3, we conduct further analysis to examine the processes driving Southern Ocean SST change using a multilinear regression (MLR) model and a thermal bipolar seesaw model adapted from Stocker and Johnsen (2003).

## 2-2: Simple models for disentangling CO<sub>2</sub> and AMOC

### 2-2-1: Multilinear Regression model

We use a MLR model to regress changes in SST onto CO<sub>2</sub> and AMOC variations:

$$SST = \alpha_I * CO_2 + \beta_I * AMOC + \gamma, (1)$$

where *SST* and *AMOC* (defined as the maximum meridional overturning streamfunction in the North Atlantic, at depths below 500 m and 20–60° N) are output from the climate models, *CO<sub>2</sub>* is the forcing used in each simulation and  $\gamma$  is the intercept. The AMOC in the analysis is normalised with respect to the temporal maximum and minimum values in each model. The CO<sub>2</sub> is also normalised with respect to the total change between 21 and 11 ka (~83 ppm). The MLR analysis is applied to the 2-D fields of the Southern Ocean SST. The same analysis is applied to the Southern Ocean SST averaged over 55–40° S. To focus on long-term climate change and reduce interannual variability, every 100-years, mean SST, AMOC, and CO<sub>2</sub> from 20 to 11 ka are used as the input for this analysis, so each dataset has 90 time-slices. While we use CO<sub>2</sub> as a representation of a gradual forcing as the input of the MLR model, we note that other forcing, such as from ice sheets and orbital changes can contribute to the warming. On the other hand, sensitivity experiments evaluating the contribution of each forcing show that they have a minor impact on Southern Ocean SST and Antarctic SAT changes between 19 and 15 ka (He et al. 2013). The results with coefficient of determination are displayed in Table 3.

### 2-2-2: Thermal bipolar seesaw model

As the MLR model does not consider the transient climate response, we construct a thermal bipolar seesaw model following Stocker and Johnsen (2003). The original thermal bipolar seesaw model is based on the energy balance between the North and South Atlantic Oceans. We add the effect of CO<sub>2</sub> on temperature, which was not considered in the original model. Thus, the thermal bipolar seesaw model in this study solves the temporal evolution of Southern Ocean SST using the following equations:

$$\frac{d\Delta SST}{dt} = \frac{\Delta SST_{eq} - \Delta SST(t)}{\tau} (2)$$



$$\Delta SST_{eq} = \alpha_2 * CO_2(t) + \beta_2 * AMOC_m(t) \quad (3)$$

where  $\Delta SST_{eq}$  is an equilibrium Southern Ocean SST (change since the LGM) expected from the  $CO_2$  and state of the AMOC at time  $t$ .  $\Delta SST(t)$  is the SST change since the LGM at time  $t$ , and  $\tau$  is the characteristic timescale of the bipolar seesaw.  $CO_2(t)$  is the  $CO_2$  concentration at time  $t$ , and is normalised with maximum and minimum values as in the MLR model. The term  $AMOC_m(t)$  represents the modes of the AMOC from the climate model outputs. When using the simulated AMOC within the bipolar seesaw model, it is assumed that the AMOC modes are binary, unlike the continuous values in the model. Based on Figure 2, we assume that the AMOC is in a strong mode ( $AMOC_m(t)=0$ ) if the AMOC is greater than 14 Sv.

At first, we conduct systematic sensitivity experiments to calculate the minimum root mean square error between the actual  $\Delta SST$  and the bipolar seesaw model. We conduct 9610 sensitivity experiments for each model within the parameter ranges shown in Table 4. The combination of parameters that gives the minimum root mean square error, along with coefficient of determination between the climate models' SST changes and bipolar seesaw models are displayed in Table 5.

### 3. Results

#### 3-1: AMOC

As AMOC variations can impact southern high latitude climate, we summarise here the transient evolution of the AMOC in the different simulations. As detailed below, the AMOC evolution is substantially affected by the freshwater forcing schemes. All simulations except for MIROC display a strong ( $\sim 20$  Sv) AMOC at the LGM (Fig. 2b), although we note that MPI-ESM and iLOVECLIM simulate a slightly weaker LGM AMOC in their sensitivity tests using the GLAC-1D ice sheet instead of ICE-6G\_C (Kapsch et al., 2022; Bouttes et al., 2023). The more vigorous LGM AMOC compared to pre-industrial is in line with the majority of the PMIP4 simulations (Kageyama et al., 2021), although it is not consistent with LGM reconstructions from multiple marine tracers (Lynch-Stieglitz et al., 2007; Bohm et al., 2015; Menviel et al., 2016).

During the period corresponding to Heinrich Stadial 1, the AMOC stays weak in MIROC and substantially declines in the iTRACE and LOVECLIM simulations, as meltwater is added into the North

Atlantic. On the other hand, in the other simulations, there is only a slight reduction in AMOC ( $\sim 1$  Sv) as the meltwater input into the North Atlantic stays below 0.05 Sv. At the transition to the Bølling-Allerød ( $\sim 14.7$  ka), three models exhibit an abrupt change from weak to strong AMOC, triggered by a rapid reduction in freshwater forcing (iTRACE and LOVECLIM) or as a response to the gradual background warming (MIROC). These simulations, featuring an AMOC strengthening, broadly agree with marine proxy records (Fig. 2b black line). On the other hand, the other three simulations (HadCM3, MPI-ESM, iLOVECLIM) display an AMOC weakening due to a substantial increase in Northern Hemisphere freshwater forcing originating from the ice sheet collapse associated with Meltwater Pulse 1a (Deschamps et al., 2012). During the Younger-Dryas (12.8–11.7 ka), iTRACE, LOVECLIM, and MIROC simulate a weakened AMOC state compared to the Bølling-Allerød, corresponding to an increase in freshwater forcing (iTRACE, LOVECLIM) or, in the case of MIROC, due to being in an oscillatory regime (Kuniyoshi et al., 2022). HadCM3 simulates a small, but gradual AMOC reduction throughout the Younger Dryas, while MPI-ESM exhibits multi-centennial AMOC variability. At 11 ka, the AMOC returns to a strong mode except for iLOVECLIM, which stays weak after the Bølling-Allerød.

270

### 271 **3-2-1: 21–18 ka (onset of warming) and 18–14.7 ka (Heinrich Stadial 1)**

272 Fig. 3 summarises the changes in Antarctic SAT (Fig. 3c-d) and Southern Ocean SST (Fig. 3e) since the LGM in all the simulations (LGM is defined as 21 ka in most models, with some exceptions because of different initialisation; 20.0 ka for iTRACE, 20.6 ka for LOVECLIM). The SAT at WDC and EDC are compared with the ice core based reconstructions from Parrenin et al. (2013) and Buizert et al. (2021). Three models (MIROC, HadCM3, MPI-ESM) exhibit a gradual  $\sim 1^\circ\text{C}$  warming between 21 and 18 ka at both WDC and EDC (Fig. 3c). The simulated EDC warming is comparable with ice core estimates, with MPI-ESM overestimating the warming at the EDC site (Fig. 4a). However, the magnitude of warming suggested by WDC ice core data ( $\sim 2^\circ\text{C}$  warming between 19.5–19 ka, Shakun et al., 2012) is not fully simulated by any of the models, with iTRACE even exhibiting slight cooling (Fig. 4a). MIROC, HadCM3 and MPI-ESM simulate a SAT increase over Antarctica and a  $0.5\text{--}1.0^\circ\text{C}$  SST increase in the Southern Ocean north of the sea ice edge, with a gradual reduction in Southern Ocean sea ice area (Figs. 3f and 4b).

283

All models exhibit a larger warming between 18 and 14.7 ka (i.e. Heinrich Stadial 1) than between 21 and 18 ka. iTRACE simulates the largest warming in SAT at WDC and EDC (+6–8°C, Figs. 3c-d), closely following the estimates from ice core data. The sharp increase in temperature in iTRACE starts at ~18 ka, corresponding to a period of major reduction in AMOC strength (Fig. 3b). The warming in MPI-ESM follows iTRACE with a 5°C warming, despite a minor reduction in AMOC strength. HadCM3 exhibits ~4°C warming at WDC and ~2°C warming at EDC, while the other models simulate a 2–4°C warming at EDC and WDC (Fig. 3c–d). iTRACE exhibits a Southern Ocean SST increase of 5°C and LOVECLIM exhibits a sharp Southern Ocean SST increase of ~3°C, in response to an AMOC reduction at ~17 ka. The other models' Southern Ocean SSTs increase by 1–2°C (Fig. 3e). Southern Ocean sea ice area exhibits the same trends as the Southern Ocean SST, with iTRACE simulating the largest sea ice area reduction of up to 40% compared to the LGM (Figs. 3f), noting that iTRACE has the largest LGM sea ice extent (Fig. 4b).

### **3-2-2: 14.7–13 ka (Bølling-Allerød) and 13–11 ka (Younger Dryas and Holocene onset)**

Three models (iTRACE, LOVECLIM, MIROC) simulate an abrupt AMOC increase at the onset of the Bølling-Allerød (Fig. 3b), and a concomitant cooling at high southern latitudes: a decrease of ~1-2°C in Antarctic SAT and Southern Ocean SST (Fig. 3c-e). iTRACE and LOVECLIM exhibit a sharp cooling in Southern Ocean SST and SAT in the early phase of the Bølling-Allerød (Fig. 3e), probably enhanced by the meltwater flux into the Southern Ocean (Menviel et al., 2011). In contrast, the three other models (HadCM3, MPI-ESM, iLOVECLIM) exhibit a warming in the early phase of the Bølling-Allerød, corresponding to their AMOC weakening. Subsequently, HadCM3 and MPI-ESM exhibit a gradual cooling over the Antarctic and Southern Ocean as the AMOC strengthens in the later part of the Bølling-Allerød (~13.5 ka). iLOVECLIM displays a rapid warming at 13.5 ka, followed by a cooling, which is explained by abrupt surface albedo changes caused by the evolving land-sea mask in the Antarctic region (Bouttes et al., 2023).

During the Younger Dryas (13–11ka), iTRACE, LOVECLIM, and MIROC simulate an AMOC weakening as well as a high southern latitude warming. iTRACE simulates a ~3–4°C increase in Southern Ocean SST, while LOVECLIM and MIROC simulate a 1°C warming. MPI-ESM exhibits multi-centennial variability associated with variations in AMOC strength. MPI-ESM and iLOVECLIM exhibit

sharp cooling in Southern Ocean SST and SAT starting at ~11.5 ka, enhanced by the meltwater flux into the Southern Ocean (Kapsch et al., 2022).

The proxy-record based estimates for total deglacial (21–11 ka) warming is 10 °C at WDC, while the EDC estimates range from 5 to 10 °C (Parrenin et al., 2013; Buizert et al., 2021). Across the simulations, 2 to 10 °C of warming is simulated over Antarctica (Fig. 3c-d). In line with the WDC and the upper range of EDC estimates, iTRACE and MPI-ESM display 8–10 °C of total warming over Antarctica. Since the LGM, the Southern Ocean sea ice edge retreats poleward by 10° latitude in models with the largest sea ice retreat (Fig. 5). The sea surface warms by up to 6 °C in the Southern Ocean near the winter sea ice edge in iTRACE, LOVECLIM, HadCM3, and MPI-ESM, while SSTs rise by ~4 °C in MIROC and iLOVECLIM (Fig. 5).

The different magnitudes of simulated warming during Heinrich Stadial 1 and the Younger Dryas across the models could be explained by the range of LGM temperature changes with respect to the pre-industrial, as the mean SAT and SST changes are different by a factor of two (Table 1). To reduce this model difference, Antarctic SATs are normalised by the temperature anomaly between LGM and the pre-industrial in Figure 6. When normalised, the simulations with a weak AMOC during Heinrich Stadial 1 show the largest warming over Antarctica (Fig. 6, left column). The normalised Antarctic SAT change at 11 ka lies between 0.6 and 0.8 × the total temperature change between the LGM and pre-industrial for five out of six models, indicating additional warming is simulated between 11 and 0 ka in the model simulations. This is different from ice core reconstructions for which the temperature at 11 ka is inferred to be comparable to the pre-industrial values (Parrenin et al., 2013; Buizert et al., 2021).

### **3-3: SST – CO<sub>2</sub> – AMOC relationship analysis**

The simulated AMOC time series display large differences across simulations due to different freshwater forcing groups, which complicates the quantification of CO<sub>2</sub> forcing and AMOC changes in driving high southern latitude temperature changes in each model. To overcome this, we examine the Southern Ocean SST trajectory against CO<sub>2</sub> forcing, and AMOC strength (Fig. 7). Fig. 7 shows that the deglacial increase in atmospheric CO<sub>2</sub> has major impacts on the Southern Ocean SST because the temperature trajectory is mostly proportional to CO<sub>2</sub> changes unless there are major AMOC changes. Temperature changes associated with changes in AMOC are superimposed on Southern Ocean SSTs;

when AMOC is weak compared to the long-term mean of the respective models (blue circles), this tends to induce warming, and vice versa. Even though the actual time series of maximum AMOC strength in each model is very different, this result suggests that high southern latitude temperature changes can be decomposed into the effects of CO<sub>2</sub> and AMOC. The relative importance of CO<sub>2</sub> and AMOC are quantified in the following subsections.

### **3-4: Results of MLR and bipolar seesaw model**

The results of the MLR model indicate that the CO<sub>2</sub> coefficients range from 1.0 to 6.5°C for the total deglacial CO<sub>2</sub> changes (Table 3). All models have a negative coefficient of AMOC (−0.3 to −2.4°C), indicating a Southern Ocean SST increase associated with AMOC weakening. The regression against Southern Ocean 2-D SST fields indicates that the CO<sub>2</sub> coefficient is mostly positive over the Southern Ocean, ranging from ~0.5 °C in the Antarctic zone where sea ice is present until 11 ka, to 2–6 °C in the Southern Ocean north of the LGM winter sea ice edge (Fig. 8). The sensitivity to the AMOC is mostly negative in the Southern Ocean, and areas of high sensitivity overlap with those of CO<sub>2</sub>, suggesting sea ice modulates the areas sensitive to both CO<sub>2</sub> and AMOC changes.

Table 5 summarises the results of the bipolar seesaw model. All models have positive CO<sub>2</sub> coefficients (2.0 to 6.0°C) and negative AMOC coefficients (−0.5 to −2.9°C), as in the MLR models. The time series simulated by the bipolar seesaw model are compared with actual SST changes and with MLR models in Fig. 9. The bipolar seesaw model succeeds in reproducing a gradual SST decrease as a result of an AMOC strengthening (e.g. gradual cooling in iTRACE and MIROC, 15–13 ka). This gradual cooling was not represented by the MLR model, which exhibits an immediate SST response to AMOC changes. With the bipolar seesaw model, the response time ranges from 100–700 years, with most models ranging from 500–700 years with the exception of LOVECLIM and iLOVECLIM (Table 5). We also fed the bipolar seesaw model with the AMOC and CO<sub>2</sub> coefficients from six different models (Table 5), but with the common inputs of CO<sub>2</sub> (Bereiter et al., 2015) and AMOC from iTRACE. The results indicate that all models would have simulated a cooling at the surface of the Southern Ocean during the Bølling-Allerød if there was an increase in the AMOC at the beginning of the Bølling-Allerød as simulated in iTRACE, LOVECLIM or MIROC (Fig. S2).

We note that the values of the CO<sub>2</sub> sensitivity from the MLR and bipolar seesaw model may include gradual forcing from other greenhouse gases, ice sheets, and orbital forcing. In addition, a sharp cooling associated with freshwater in the Antarctic Ocean was not represented because both models, MLR and bipolar seesaw, do not consider meltwater in the Southern hemisphere (~14.5 ka of iTRACE and LOVECLIM, ~11.5 ka of MPI-ESM and iLOVECLIM)

### **3-5: Other Southern Ocean climate variables**

We further analyse Antarctic Bottom Water transport (defined as the minimum global meridional overturning streamfunction, at depths below 3000 m and 60° S) as an indicator of Southern Ocean meridional circulation, and 850 hPa zonal mean winds over the Southern Ocean (zonal mean winds averaged over 65–40° S), to analyse the potential impact on deglacial CO<sub>2</sub> changes, which is prescribed in the experiments. We focus on the onset of deglaciation (21–18 ka) and the initial significant increase in CO<sub>2</sub> (during Heinrich Stadial 1, 18–15 ka). Antarctic Bottom Water (Fig. 10b) at the LGM ranges from 10 to 30 Sv among the six models and stays relatively constant between 21 and 18 ka. In the subsequent period (18–15 ka), iTRACE exhibits a gradual decline in Antarctic Bottom Water, in phase with Southern Ocean SST changes (Fig. 10d). LOVECLIM and MPI-ESM exhibit a gradual decline in Antarctic Bottom Water (~5 Sv), while three other models (MIROC, HadCM3, iLOVECLIM) exhibit a small reduction in or constant Antarctic Bottom Water formation. Thus, while all models simulate Southern Ocean SST warming and sea ice retreat during Heinrich Stadial 1, the trends in Antarctic Bottom Water formation differ. In addition, the Antarctic Bottom Water changes do not depend on the AMOC evolution and thus freshwater forcing groups (Fig 10a–b). The zonal winds over the Southern Ocean exhibit slight change between 21 and 18 ka, apart from MIROC and MPI-ESM, which both exhibit a slight weakening (Fig. 10c). Between 18 and 15 ka, the zonal winds continue to decline in MIROC and MPI-ESM, and start to decline in iTRACE and LOVECLIM. Little changes in zonal winds are simulated in iLOVECLIM, while HadCM3 exhibits a ~10% strengthening.

Subsurface ocean temperatures south of 60° S at depths of around 500 m (Fig. 10e) exhibit an increase during Heinrich Stadial 1 in 4 of the 6 simulations, with the largest warming (1.2°C and 0.8°C) simulated by the two simulations which exhibited the largest SST increase (iTRACE and MPI-ESM).

During the Bølling-Allerød (15–13 ka), iTRACE and MIROC exhibit a gradual sub-surface temperature decrease while HadCM3 and MPI-ESM exhibit continuous warming, as per the SST changes in the respective models. iLOVECLIM and LOVECLIM exhibit small changes ( $<0.5^{\circ}\text{C}$ ) in the total sub-surface temperature. Abrupt subsurface warming in iTRACE (~14 ka) and LOVECLIM (14.8–14.2 ka) coincide with Southern Ocean SST reduction, suggesting that this results from enhanced Southern Ocean stratification as a response to Southern Ocean meltwater input (Menviel et al., 2011; Lowry et al., 2018).

### **3-6: Additional freshwater experiments on Heinrich Stadial 1 SO warming in MIROC and HadCM3**

We additionally show two simulations run with the MIROC and HadCM3 models to assess the impact of freshwater forcing on southern high latitude climate during Heinrich Stadial 1. As a reminder, MIROC and HadCM3 are assigned to different freshwater groups (Fig. 2). In the MIROC simulations, the freshwater forcing during Heinrich Stadial 1 is increased to 0.1 Sv or 0.2 Sv between 18 and 15.5 ka (Figure 11a, red and orange lines) instead of 0.03 Sv in the standard simulation. This larger meltwater input further weakens the AMOC (Fig. 11a) and leads to an additional  $1^{\circ}\text{C}$  SST increase in the Southern Ocean compared to the standard simulation (Fig. 11d). The  $1^{\circ}\text{C}$  warming in response to the AMOC reduction of ~5 Sv is a greater response than is produced by the MLR and bipolar seesaw models. In the HadCM3 simulations, a North Atlantic freshwater flux of ~0.2 Sv during Heinrich Stadial 1 (similar to Trace-21ka A, Liu et al., 2009) reduces the AMOC by 15 Sv (Fig. 11e blue lines), and induces an additional  $\sim 1^{\circ}\text{C}$  increase in Southern Ocean SST compared to the standard simulation (Fig. 11h). The simulated Heinrich Stadial 1 warming in HadCM3 is consistent with both MLR and bipolar seesaw models (Tables 3 and 5). The results from the MIROC and HadCM3 sensitivity experiments show that the simulated warming during Heinrich Stadial 1 can be twice as strong with an AMOC shutdown compared to the standard simulation of each model. As in the LOVECLIM Heinrich stadial 4 simulation (Figure S2; Margari et al. 2020), southern high latitude temperatures do not necessarily respond linearly to changes in AMOC strength, and MLR models assume a linear temperature response to the AMOC.

## **4. Discussion**

### **4-1: Onset of deglacial warming**

The climate forcing in the early deglaciation primarily comes from insolation due to obliquity and precession changes (Fig. 1a), which leads to an increase in spring to summer insolation south of 60 °S (Fig. S3). Ice core data suggest that the onset of deglacial warming at WDC was earlier than the increase in CO<sub>2</sub>, and this early deglacial warming has been suggested to result from an AMOC reduction (Shakun et al., 2012) or local insolation changes (WAIS project members, 2013). However, simulated early warming is smaller than inferred from proxy records. Three models (MIROC, HadCM3, MPI-ESM) exhibit a small warming (~ 0.5°C) between 21 and 18 ka (Fig. 4a) in both West and East Antarctica, as well as at the surface of the Southern Ocean, primarily in the Pacific sector (Fig. 4b), consistent with proxy records (Moy et al., 2019; Sikes et al., 2019; Moros et al., 2021) and a previous modelling study (Timmermann et al., 2009). The other models show a slight cooling (iTRACE) or little change (LOVECLIM and iLOVECLIM).

The first explanation for the differences in the simulated temperature change between 21 and 18 ka relates to Southern Ocean sea ice at the LGM. MIROC, HadCM3 and MPI-ESM have less LGM summer sea ice than other models, which may lead to a relatively high sensitivity to increased insolation during austral spring to summer, causing significant warming with sea ice retreat (Timmermann et al., 2009; Roche et al., 2011). If the LGM Southern Ocean sea ice extent is extensive, the increase in insolation primarily south of 60 °S (Fig. S3) does not warm the Southern Ocean as much because of high sea ice albedo. Although the local insolation changes are the likely cause of the early warming simulated in some of the models, the addition of freshwater could contribute to the AMOC weakening. For example, the consideration of an additional freshwater flux from the Fennoscandian ice sheet in the freshwater forcing prior to 18 ka, suggested by Toucanne et al. (2010), would weaken the AMOC and lead to a more pronounced warming in the southern high latitudes.

Another model-data difference is in the early warming rates between West and East Antarctica. The data from WDC suggest there was significant warming in West Antarctica, while a less significant change in East Antarctica is suggested by EDC records. In contrast, the models simulate similar warming rates in both West and East Antarctica (Fig. 4a), suggesting the models may underestimate the spatial heterogeneity in West and East Antarctic warming. This might be attributed to the Antarctic ice sheet history prescribed in the experiments, where both ICE-6G\_C and GLAC-1D have minor surface elevation



changes at WDC in the early deglaciation (Fig. 1d). Buizert et al. (2021) used the MIROC and HadCM3 models to show that the uncertainty in Antarctic ice sheet height affects SAT due to the impact of lapse rates ( $\sim 1^\circ\text{C}$  warming per 100 m altitude reduction). This might suggest that the lower surface elevations at WDC, related to ice sheet terminus retreat 20–15 ka in the Amundsen Sea (Bentley et al. 2014), contributed to the early deglacial warming primarily in West Antarctica. The coarse resolution of the atmospheric models (2.5 to 5.6 degrees horizontally) may impact the warming contrast between East Antarctica (EDC ice core site) and West Antarctica (WDC ice core site) through an inherent smoothing of the surface topography of the Antarctic ice sheet and the associated impact on the atmospheric circulation (Buizert et al., 2021). In addition, the relatively coarse resolution of the ocean models (1 to 3 degrees), may impact AMOC sensitivity to iceberg and freshwater fluxes in the North Atlantic (Condrón and Winsor 2012), or the impact of mesoscale processes in the Southern Ocean (Morrison et al., 2013) and their response to the deglaciation.

Uncertainty in Antarctic ice sheet topography could also explain some model-proxy record differences during the early Holocene, where simulations indicate that an additional warming occurs after 11 ka (Fig. 6). This is different from ice core data (Fig. 4) and global mean ocean temperature (including deep-sea temperature) estimated from noble gases in ice cores, which suggests that temperatures reach Holocene levels at the end of Younger Dryas (Bereiter et al., 2018). The decrease in surface elevation of the Antarctic ice sheet after 11 ka (Fig. 1e) may contribute to the Holocene warming. It would be valuable to assess the uncertainties from ice sheet reconstructions, as new reconstructions have been published (e.g., Gowan et al., 2021), and different LGM ice sheets can induce different AMOC variabilities (Prange et al., 2023; Masoum et al., 2024).

#### **4-2: Rate of temperature changes**

Heinrich Stadial 1 ( $\sim 18$ – $14.7$  ka) exhibits major warming in all models because of the  $\text{CO}_2$  increase, with the total warming being dependent on the sensitivity of each model to  $\text{CO}_2$ , and to AMOC changes. In turn, the deglacial AMOC evolution is dictated by the glacial meltwater input, as shown in additional sensitivity experiments performed with MIROC and HadCM3 (Fig. 11). Among the six models, iTRACE simulates the largest warming during Heinrich Stadial 1, with an Antarctic SAT increase of 6– $8^\circ\text{C}$  and a rise in Southern Ocean SST of 4– $5^\circ\text{C}$ . While Antarctic SAT matches ice-core data, simulated

479 Southern Ocean SST is larger than the SST stack (Fig. 3e). Five models besides iTRACE simulate a  
480 Southern Ocean SST change that compare well with the SST stack, but these five models underestimate  
481 Antarctic SAT. This indicates that the different magnitudes of warming between Southern Ocean SST  
482 and Antarctic SAT are not fully reconciled in the physics-based models. While iTRACE exhibits the  
483 largest cooling of global mean SAT at the LGM compared to pre-industrial (7.3°C, compared to the six-  
484 model mean of 5.3°C), the ECS of iTRACE (3.6°C) is not the highest among the six models; instead,  
485 MIROC4m has the highest ECS despite weaker deglacial warming (Table 1). We examine the relationship  
486 between ECS and the LGM global mean SAT changes using multi-model PMIP3 and PMIP4 simulations  
487 (Fig. S4). We find a weak negative correlation ( $-0.06$ ) between the ECS and global mean LGM SAT  
488 changes, and the local SAT change in the individual climate models can vary by about a factor of two  
489 even with the same ECS. A substantial asymmetry between warm and cold climates has been identified  
490 in previous studies because of the presence of continental ice sheets, ocean dynamics, and cloud feedback  
491 (Yoshimori et al., 2009; Zhu and Poulsen, 2021). Hence, understanding the mechanisms and amplitude  
492 of cooling in the LGM simulations will contribute to a better understanding of multi-model differences  
493 in the deglacial warming.

494 The sensitivity to AMOC ranges between  $-0.5$  and  $-2.9^{\circ}\text{C}$  based on the analysis using the thermal  
495 bipolar seesaw model (Table 5). A multi-model study comparing freshwater hosing experiments of 11  
496 climate models (including LOVECLIM, MIROC, and HadCM3 used in this study) under LGM climate  
497 shows that most models exhibit warming in the Southern Ocean (Kageyama et al., 2013). However, the  
498 simulation length in that study is less than 420 years. In this study, we estimated that the bipolar seesaw  
499 operates on a timescale of  $\sim 500\text{--}700$  years. Thus, longer simulations are needed to evaluate the extent of  
500 the climate response at high southern latitudes.

501 The MLR and thermal bipolar seesaw models in this study include several assumptions. Firstly,  
502 as the gradual forcing is represented only by the  $\text{CO}_2$  concentration, they do not consider the effect from  
503 retreating ice sheets, meltwater flux in the Southern Ocean, or insolation changes explicitly. Other  
504 forcings could be included in the  $\text{CO}_2$  or AMOC coefficients in this analysis. For instance, insolation  
505 change in boreal summer is positively correlated with  $\text{CO}_2$ ; both exhibit a gradual increase (Fig. 1a-b).  
506 Antarctic and Northern Hemisphere ice sheet changes could impact Southern Ocean SST (Abe-Ouchi et

al., 2015). This may explain the CO<sub>2</sub> coefficients from the MLR and bipolar seesaw model being higher than expected from the ECS value. On the other hand, the AMOC sensitivity of the LOVECLIM model is low compared to the 1.5°C Southern Ocean SST increase found in the simulation of Heinrich stadial 4 (Margari et al. 2020, Fig. S5), and the CO<sub>2</sub> coefficient is quite high, potentially implying a poor separation or substantial interconnectivity of the two factors.

#### 4-3: Freshwater forcing and temperature changes in southern high latitudes

As shown here, the deglacial AMOC variations are quite different amongst the simulations. Only those that display an AMOC increase at the end of Heinrich Stadial 1 can capture a cooling trend at the Bølling-Allerød (corresponding to the Antarctic Cold Reversal) consistent with ice-core data (iTRACE, LOVECLIM, MIROC). In comparison to previous transient simulations of the last deglaciation, the representation of the duration of the Antarctic Cold Reversal has improved, as it was previously simulated as too short (Lowry et al., 2018). On the other hand, individual climate model simulations that are forced with a large Northern Hemisphere meltwater pulse consistent with ice sheet reconstructions do not simulate an increase in the AMOC at the Bølling-Allerød (Ivanovic et al., 2016; 2018; Kapsch et al., 2022; Bouttes et al., 2023; Snoll et al., 2024). Freshwater forcing in the Northern Hemisphere and associated reduction in the AMOC led to Antarctic warming during Heinrich Stadial 1 in sensitivity experiments with individual forcing (He et al., 2013) and sensitivity experiments with freshwater forcing (Figure 11).

A comparison of the six models reveals that capturing phase changes in the AMOC is necessary to simulate warming or cooling trends at southern high latitudes. This is also supported by results from the bipolar seesaw model simulations forced with a common AMOC (Fig. S2). While MIROC simulates a rapid increase in the AMOC at the Bølling-Allerød transition with a continuous freshwater flux (Fig. 2), a 50% greater (i.e. 1.5 ×) freshwater forcing produces a weak AMOC throughout the last deglaciation (Obase et al., 2021). Thus, the simulated temperature changes at southern high latitudes are sensitive to freshwater forcing in the Northern Hemisphere.

However, the timing and magnitude of meltwater input inferred from ice sheet reconstructions conflicts with the meltwater forcing needed to obtain a deglacial climate evolution in agreement with proxy records. This so-called meltwater paradox (Ivanovic et al., 2018; Snoll et al., 2024) is present for

major periods of the last deglaciation including the Bølling-Allerød transition and Heinrich Stadial 1. This highlights a need for more accurately constrained freshwater forcing scenarios (and then envelope of uncertainty), and a need to assess the sensitivity of climate models to freshwater forcing (including the reduction of climate model biases impeding the correct sensitivity). We also note that the routing location of meltwater input (Roche et al., 2010; He et al., 2020) and the method for implementing of iceberg and meltwater discharges into the ocean (Schloesser et al., 2019; Love et al., 2021) may induce different AMOC changes.

In addition, freshwater forcing from the Antarctic ice sheet can enhance the Antarctic Cold Reversal, as found in iTRACE (~14.2 ka) and LOVECLIM (~14.7 ka), with a sharp cooling in Southern Ocean SST and Antarctic SAT primarily in WDC. This is caused by the intensified stratification in the Southern Ocean (Menviel et al., 2010; 2011), which induces significant warming in the subsurface and contributes to further Antarctic ice mass loss (Golledge et al., 2014). As ice core data does not exhibit such sharp cooling events as compared to climate model simulations (Fig. 3), this may provide some constraints on the extent and duration of freshwater forcing from the Antarctic ice sheet.

#### **4-4: Implications for climate system changes at high southern latitudes**

Reconstructions have suggested that changes in Southern Ocean circulation, probably driven by wind changes, were important for the modulation of Southern Ocean CO<sub>2</sub> outgassing during the deglaciation. Proxy records suggest there was an enhanced opal flux during Heinrich Stadial 1, which could reflect increased upwelling in the Southern Ocean due to changes in Southern Hemispheric westerlies (Anderson et al., 2009), and poleward shift of the Southern Hemisphere Westerlies across the deglaciation (Gray et al., 2023). Proxies also suggest an increase in deep and intermediate-depth Southern Ocean ventilation (Skinner et al., 2010, Burke et al., 2011), increasing intermediate-depth pH in the Southern Ocean during Heinrich Stadial 1 (Rae et al., 2018). It has been suggested that stronger or poleward-shifted Southern Hemisphere Westerlies and/or enhanced Antarctic Bottom Water formation during Heinrich Stadial 1 would indeed enhance Southern Ocean CO<sub>2</sub> outgassing and lead to an atmospheric CO<sub>2</sub> increase (Menviel et al., 2014; Menviel et al., 2018).

In contrast, in the present study, most models show very little change or a gradual weakening in the Southern Hemisphere Westerlies throughout the deglaciation and there is little latitudinal migration. Only HadCM3 simulates a strengthening in the Westerlies during Heinrich Stadial 1. This relative inertia in the wind conditions may be influenced by biases in the Southern Hemisphere Westerlies in pre-industrial simulations. Additional research could study in more detail the changes in regional strength and their relation to other climatic variables (Rojas et al., 2009; Sime et al., 2013).

In addition, no model exhibits an increase in Antarctic Bottom Water formation, which could contribute to the upwelling of carbon-rich waters and CO<sub>2</sub> outgassing from the Southern Ocean. Instead, the long-term Antarctic Bottom Water weakening driven by Southern Ocean warming and sea ice melt is consistent with previous analyses of deglaciation experiments (Marson et al., 2016). While it has been suggested that larger Southern Ocean sea ice extent would lead to an atmospheric CO<sub>2</sub> decrease at the LGM (Ferrari et al., 2014; Marzocchi et al., 2020, Stein et al., 2020), few models simulate significant changes in atmospheric CO<sub>2</sub> due to Southern Ocean sea ice change (Gottschalk et al., 2019). These physical changes still need to be reconciled with processes put forward to explain the deglacial trends in atmospheric CO<sub>2</sub>, for example, by running coupled climate-carbon simulations.

Finally, we also find that changes in subsurface ocean temperature in the Southern Ocean, one of the critical factors impacting the retreat of the Antarctic ice sheet, display significant differences across the simulations. This could be related to different ECS or freshwater forcing in the Southern Ocean, and should also be investigated in future work to quantify uncertainties in subsurface ocean temperature changes. Model-dependent subsurface ocean temperature change is one source of uncertainty in projecting future Antarctic ice sheet mass loss (Serrousi et al., 2020). In contrast to the present simulations of the last deglaciation, which prescribe the Antarctic ice sheet history, climate variability occurring during the deglaciation can impact the Antarctic ice sheet, which can act as feedback to Southern Ocean climate via meltwater input from the Antarctic ice sheet (Menviel et al., 2010; Golledge et al., 2014; Clark et al., 2020). Hence, further coupled climate and ice sheet modelling studies are needed to improve our understanding of climatological and glaciological processes and to evaluate model performance under a warming climate and rising sea levels (Gomez et al., 2020).

## 5. Conclusion

In our multi-model analysis of transient deglacial experiments, the early increase in Antarctic SAT is weakly simulated or absent. The multi-model difference could be related to divergence in LGM sea ice extent, which may affect model sensitivity to insolation change, or to a slight reduction in the AMOC in response to low levels of freshwater input from the Northern Hemisphere ice sheets.

In addition, the different warming rates between West and East Antarctica inferred from ice core records are not reproduced by the transient simulations. In all models, a major warming occurs at southern high latitudes between 18 and 15 ka in response to increased CO<sub>2</sub> concentration. The multi-model analysis and sensitivity experiments further suggest that the AMOC reduction during Heinrich Stadial 1, which is associated with increased freshwater flux in the North Atlantic, contributes to a larger warming in southern high latitudes, in agreement with high southern latitude proxy records, even though no simulation can reproduce both the amplitude of Southern Ocean SST and Antarctic SAT changes simultaneously. The bipolar seesaw model indicates that all models have a bipolar seesaw response, and that an abrupt AMOC increase at the end of Heinrich Stadial 1 is necessary to simulate the high southern latitude cooling during the Bølling-Allerød (corresponding to the Antarctic Cold Reversal).

The simulations exhibit little change in winds over the Southern Ocean and meridional circulation in the Southern Ocean, raising questions about what processes could have contributed to enhanced CO<sub>2</sub> outgassing from the Southern Ocean. This indicates the necessity for future climate system modelling studies to quantify the sequence of deglacial climate changes and atmospheric CO<sub>2</sub> increase.

## **Acknowledgements:**

We thank the three anonymous referees for their valuable comments which have substantially improved our paper. TO, AAO, TV and WLC acknowledge funding from JSPS Kakenhi 17H06104, 17H06323, and JPJSBP120213203. TO was also supported by JPMXD0722680395 and JSPS Kakenhi 24H00026. We acknowledge discussions at PAGES-QUIGS T5–T0 workshops, supported by INQUA Terminations Five to Zero (T5–T0) Working Group (Project #2004). LM acknowledges funding from Australian Research Council (ARC) grants FT180100606 and SR200100008. UM and MK acknowledge funding by the German Federal Ministry of Education and Research as a Research for Sustainability Initiative through the PalMod project (grant nos. 01LP1915C, and 01LP1917B). The MLR analysis used

scikit-learn library of Python 3.7. The figures were created using Generic Mapping Tool (GMT version 4 and 6).

**Data availability:**

Model data supporting our findings will be archived at Zenodo. Original model data is upon request for authors from each modelling group.

**Code availability:**

The bipolar seesaw model and the MLR model used in this study can be shared upon request.

**Author contribution:**

TO, LM, and AAO conceived the study. TO, LM, TV, BS analysed the data. TO, LM, AAO, TV, RI, and BS wrote the manuscript with input from all co-authors.

**Competing interests:**

Laurie Menviel is a member of the editorial board of Climate of the Past, but otherwise all authors declare that they have no conflict of interest.

**References:**

Name	Climate model name	Equilibrium Climate Sensitivity (ECS) [K]	Global mean LGM SAT anomaly [K]	References
iTRACE	iCESM1.3	3.6	7.3	Tierney et al., (2020)
LOVECLIM	LOVECLIM	2.8	4.2	McDougall et al., (2020), Goosse et al., (2010)
MIROC	MIROC4m	3.9	4.5	Chan and Abe-Ouchi, (2020)
HadCM3	HadCM3B	2.7	6.1	Kageyama et al., (2021)
MPI-ESM	MPI-ESM-CR P2		6.1	Kapsch et al., (2022)
iLOVECLIM	iLOVECLIM	2.0	3.5	Bouttes et al., (2023)

**Table 1:** Summary of climate models analysed in this study. Note that the ECS for MPI-ESM (model version MPI-ESM-CR P2) has not been calculated.

Name	Freshwater scheme	GHGs	Ice sheets	References
iTRACE	TraCE-like	PMIP4	ICE-6G_C	He et al., 2019; 2021
LOVECLIM	TraCE-like, spatially uniform to the North Atlantic	Kohler et al., 2017	ICE-5G	Menviel et al., 2011
MIROC	ICE-6G_C with adjustment, spatially uniform to the North Atlantic	PMIP4	ICE-5G (LGM fix)	Obase and Abe-Ouchi 2019; Obase et al., 2021
HadCM3	ICE-6G_C	PMIP4	Ice-6G_C	Ivanovic et al., 2018; Snoll et al., 2022
MPI-ESM	ICE-6G_C	Kohler et al., 2017	Ice-6G_C	Kapsch et al., 2022
iLOVECLIM	ICE-6G_C	PMIP4	Ice-6G_C	Bouttes et al., 2023

636 **Table 2:** Summary of the experimental design used in the transient deglacial simulations. PMIP4 in the  
637 column *GHGs* indicates they use three greenhouse gases reconstructions (CO<sub>2</sub>, CH<sub>4</sub>, N<sub>2</sub>O) in PMIP4  
638 protocol paper (Ivanovic et al., 2016).

	CO <sub>2</sub> coefficient [K/83 ppm]	AMOC coefficient [K/(normalised AMOC)]	Coefficient of Determination
iTRACE	6.5	−2.4	0.90
LOVECLIM	4.1	−0.4	0.91
MIROC	1.4	−0.5	0.81
HadCM3	3.3	−1.4	0.95
MPI-ESM	3.1	−1.2	0.90
iLOVECLIM	1.0	−1.4	0.56



640 **Table 3:** Results of the MLR model for Southern Ocean SST.

Parameter [unit]	Range
CO <sub>2</sub> coefficient $\alpha$ [K/83 ppm]	1.0–7.0, every 0.2
AMOC coefficient $\beta$ [K/(normalised AMOC)]	0.0–3.0, every 0.1
Response timescale $\tau$ [year]	100–1000, every 100

641 **Table 4:** Parameter ranges in the thermal bipolar seesaw model.

	CO <sub>2</sub> coefficient [K/83 ppm]	AMOC coefficient [K/(normalised AMOC)]	Response timescale [year]	Coefficient of determination
iTRACE	6.0	−2.9	500	0.97
LOVECLIM	4.4	−0.6	300	0.94
MIROC	2.4	−0.9	600	0.97
HadCM3	4.8	−1.3	700	0.99
MPI-ESM	3.4	−1.4	500	0.95
iLOVECLIM	2.0	−0.8	100	0.54

642 **Table 5:** Results of the bipolar seesaw model for Southern Ocean SST

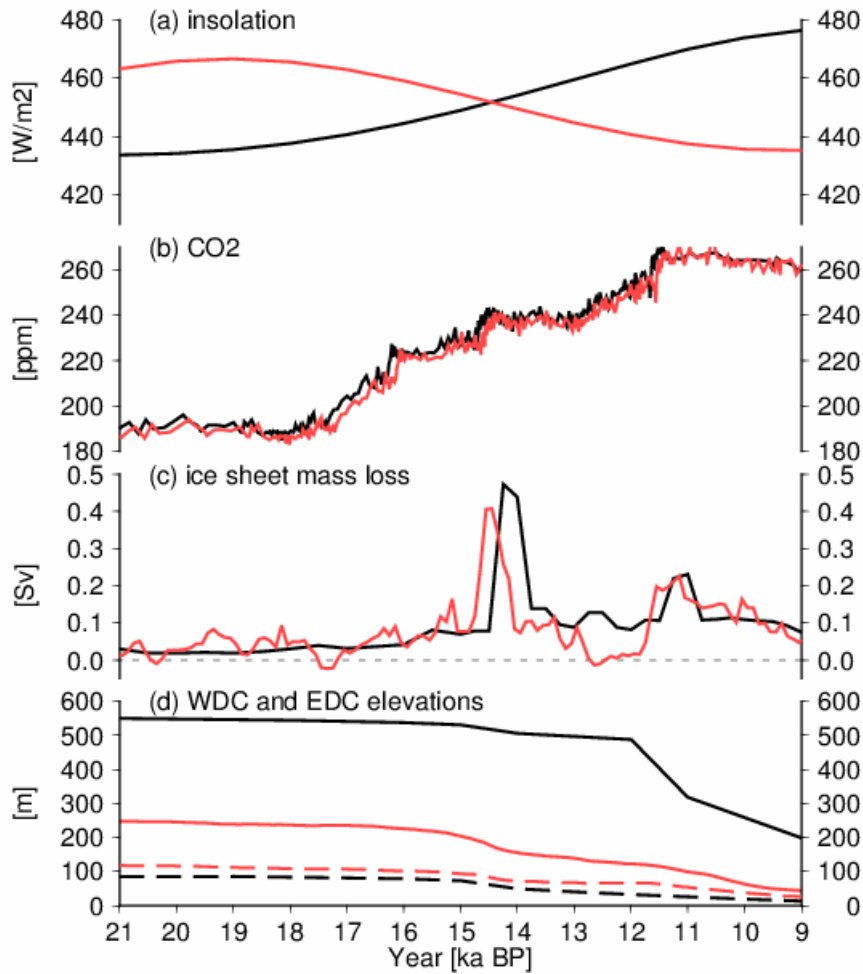


**Figure 1:** Forcing of the last deglaciation. (a) Insolation based on Berger (1978). Black: 65°N July, red: 65°S January, (b) CO<sub>2</sub>. Black: Bereiter et al., (2015), red: Kohler et al., (2017), (c) freshwater forcing in the NH from ICE-6G\_C (black lines) and GLAC-1D (red lines), (d) Elevation change at WDC (bold lines) and EDC (dashed lines) from ICE-6G\_C (black lines) and GLAC-1D (red lines).

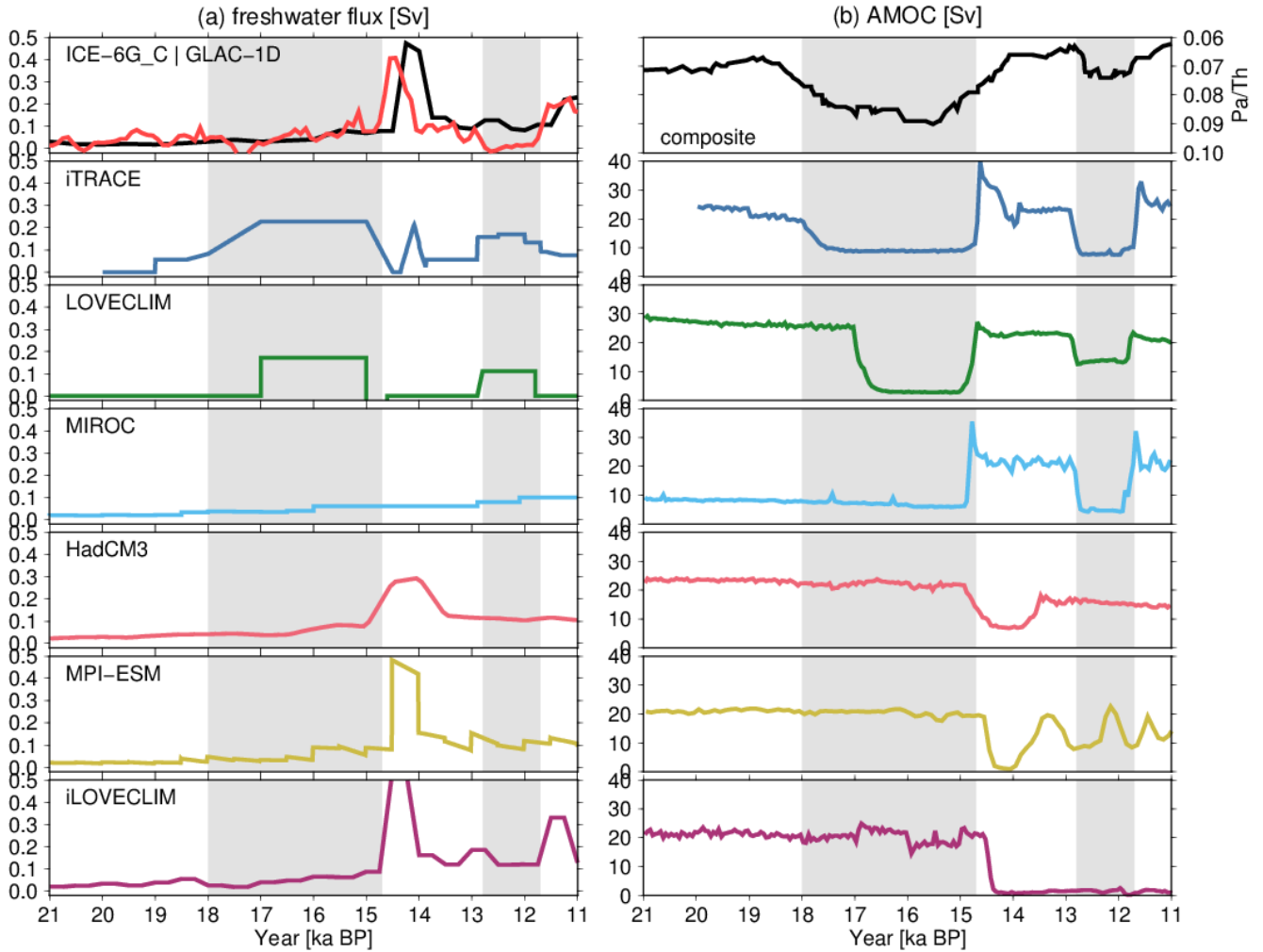


**Figure 2:** (a) Freshwater forcing (total value in the NH) and (b) simulated AMOC time series. The top panels indicate the freshwater flux from ice sheet reconstructions (black indicates ICE-6G\_C and red indicates GLAC-1D) and composite  $^{231}\text{Pa}/^{230}\text{Th}$  in the North Atlantic, retrieved from Ng et al., (2018). The top three model panels correspond to the first group with freshwater forcing adjusted to reproduce large-scale AMOC variability, and the bottom three model panels correspond to the second group with freshwater forcing consistent with the reconstructed ice volume changes. The grey shading indicates Heinrich Stadial 1 (18–14.7 ka) and the Younger Dryas (12.8–11.7 ka), respectively, and the period in between corresponds to the Bølling-Allerød (14.7–12.8 ka).

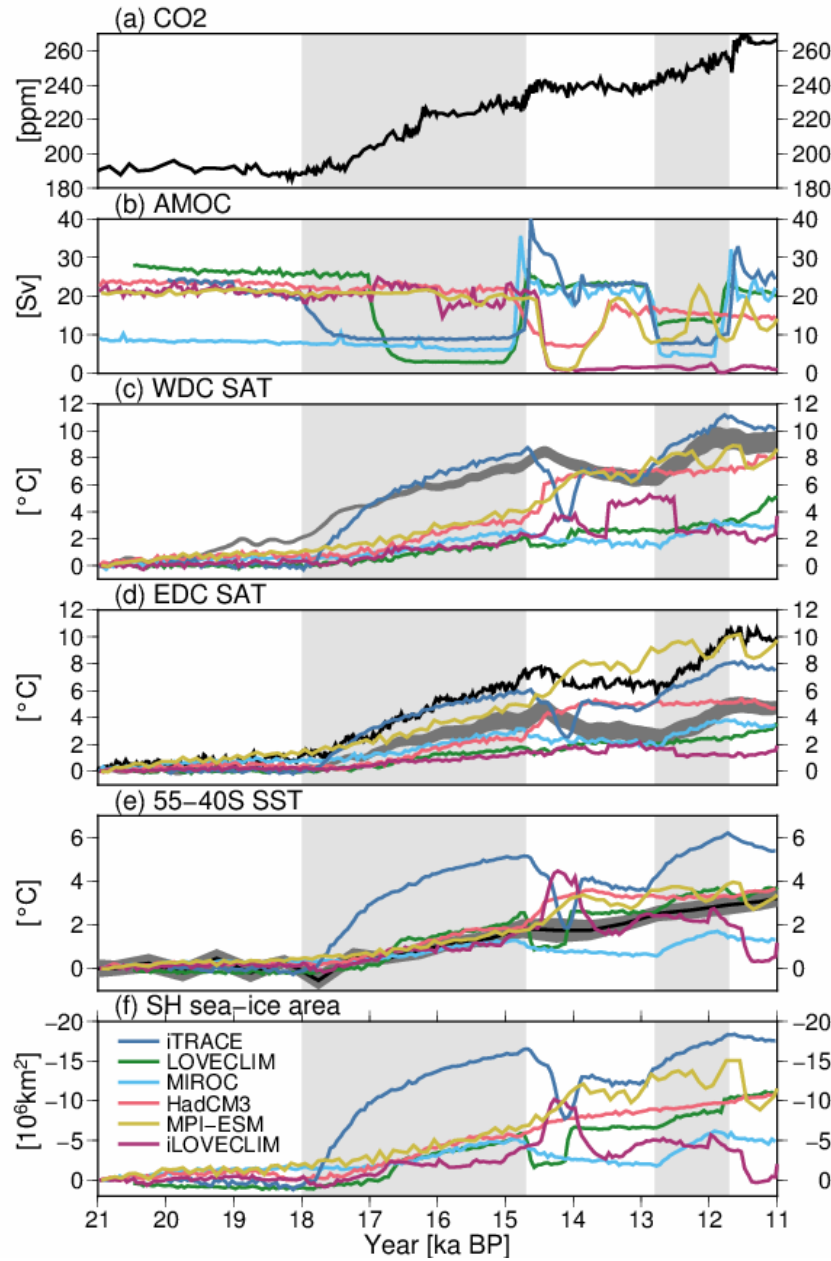
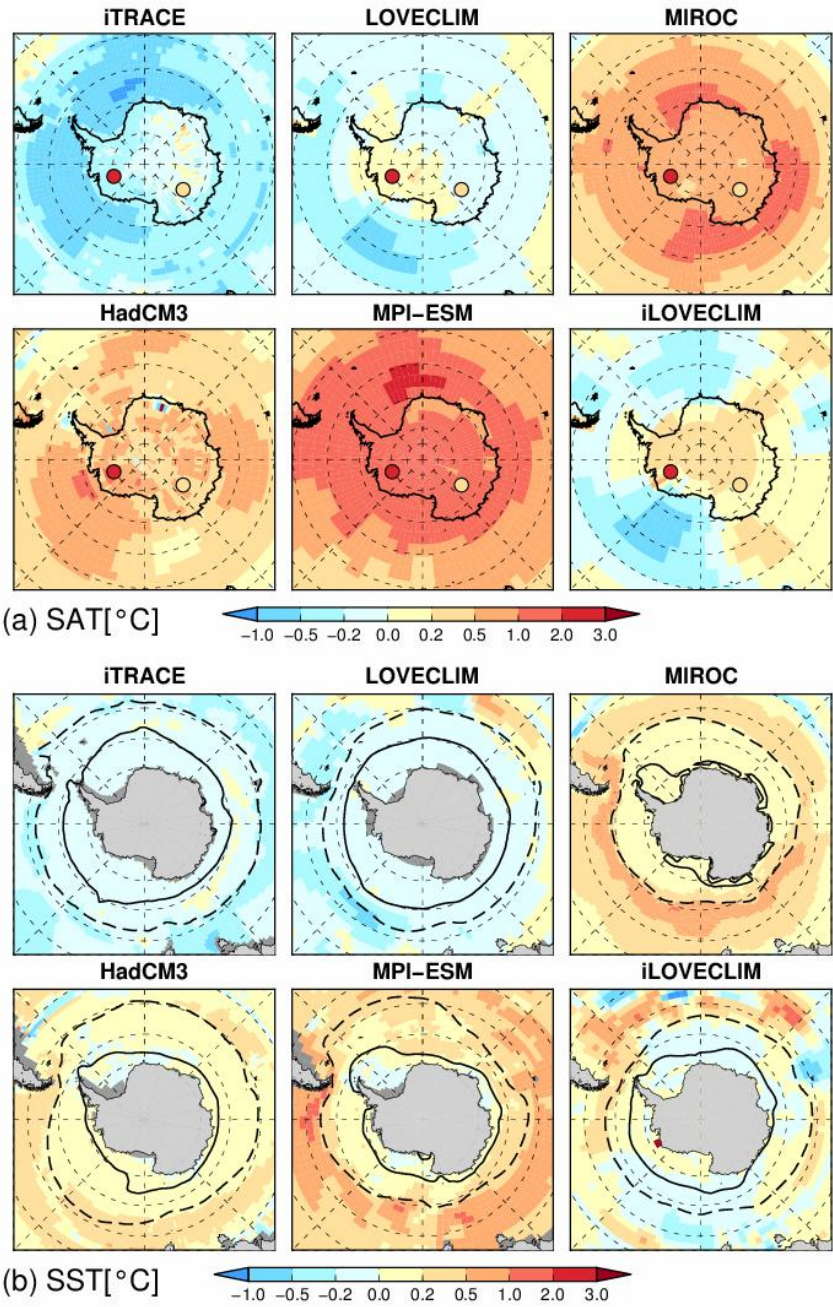


**Figure 3:** Time series of (a) atmospheric CO<sub>2</sub> (Bereiter et al., 2015) and (b) simulated AMOC, (c–d) SAT at WDC and EDC, (e) Southern Ocean SST (zonal mean SST in the latitude band 55–40°S), (f) Southern Ocean sea ice area in the transient simulations. The SAT, SST and sea ice area indicate changes since the LGM. The grey lines in (c–d) represent reconstructions from Buizert et al., (2013), and the black line in (d) represents reconstructions from Parrenin et al., (2013). The black lines and grey shades in (e) indicate the Southern Ocean SST stack and its standard error, respectively, as derived by Anderson et al., (2020).

664 The vertical grey shading indicates Heinrich Stadial 1 (18–14.7 ka) and the Younger Dryas (12.8–11.7  
665 ka), respectively, and the period in between corresponds to the Bølling-Allerød (14.7–12.8 ka).

666

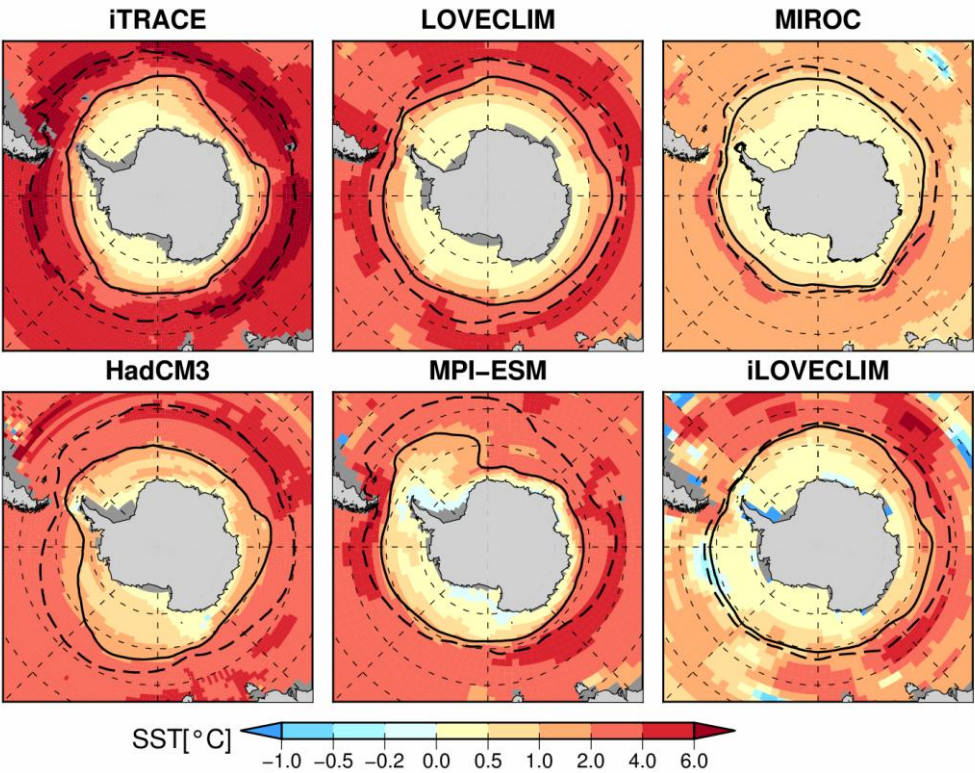


667



668 **Figure 4:** (a) SAT and (b) SST anomalies at 18 ka compared to the LGM. The coloured circles in (a)  
 669 represent 18 ka-LGM SAT change based on ice core data (Parrenin et al., 2013), and the bold and dashed  
 670 lines in (b) represent LGM austral summer and winter sea ice extent (85 and 15% annual-mean sea ice  
 671 concentration), respectively.

672



673  
 674 **Figure 5:** SST anomalies at 11 ka compared to the LGM. The bold and dashed lines indicate LGM and  
 675 11 ka sea ice extent (15% sea ice concentration), respectively.

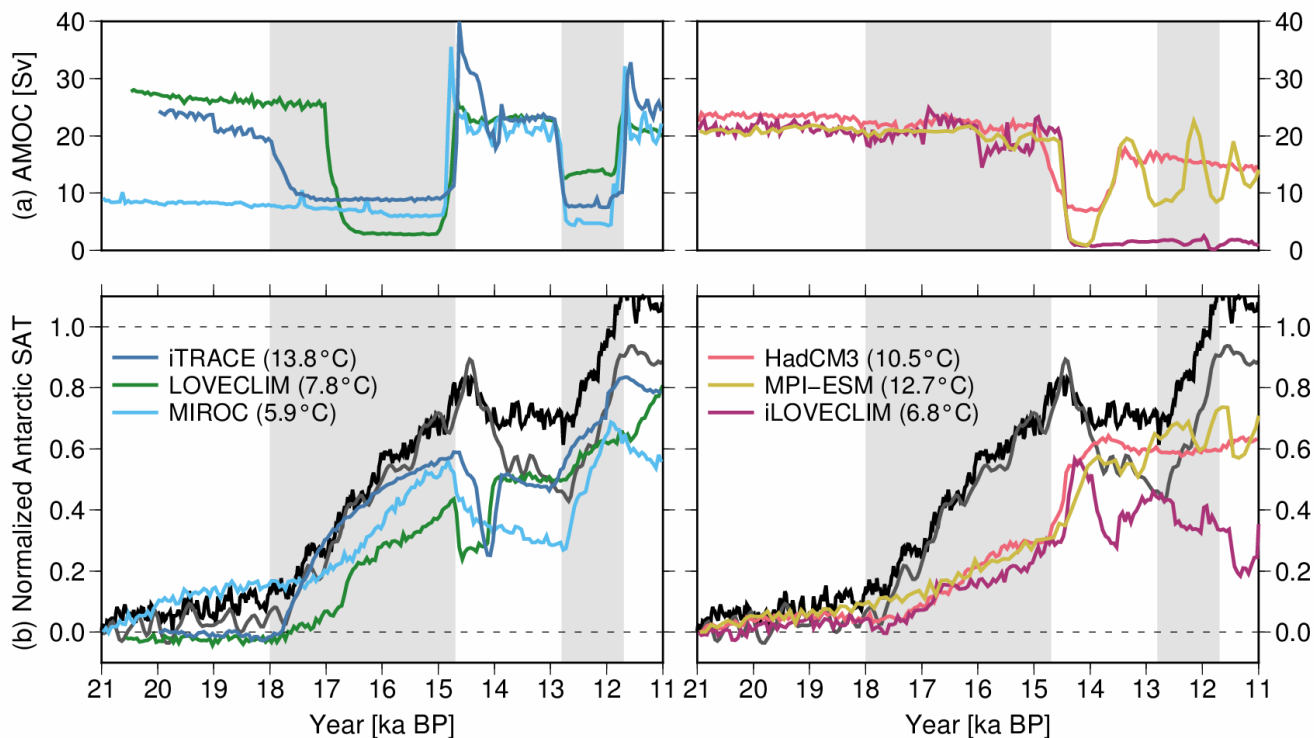
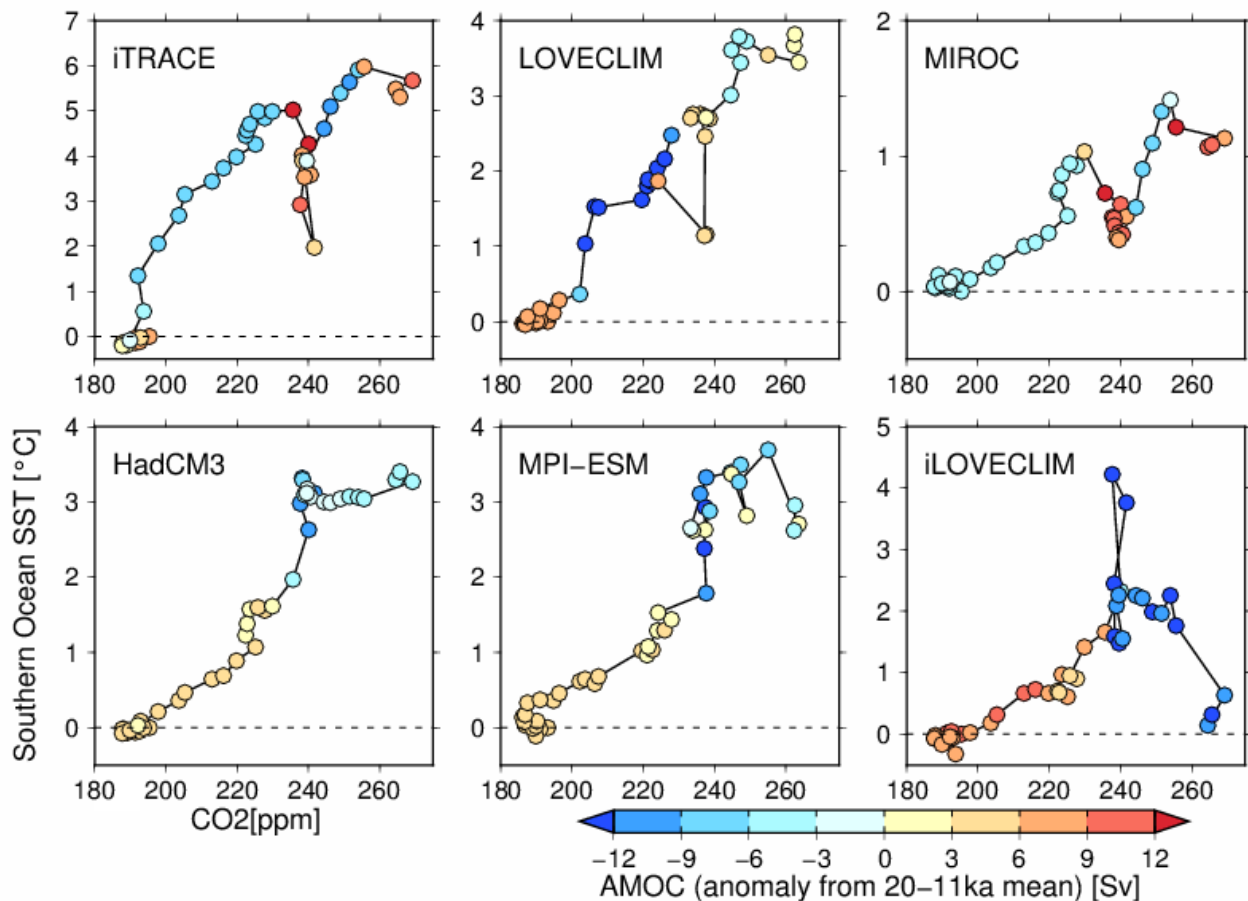


**Figure 6:** AMOC and normalised Antarctic SAT, with respect to the difference between the pre-industrial and LGM. The actual pre-industrial and LGM differences are indicated in parentheses. The left panels show three simulations with weak AMOC during Heinrich Stadial 1, and the right show strong AMOC during Heinrich Stadial 1, respectively. The grey and black lines in (b) are normalised Antarctic SAT recorded by EDC ice based on Parrenin et al., (2013) and Buizert et al., (2021), respectively. The vertical grey shading indicates Heinrich Stadial 1 (18–14.7 ka) and the Younger Dryas (12.8–11.7 ka), respectively, and the period in between corresponds to the Bølling-Allerød (14.7–12.8 ka).



684

685 **Figure 7:** Relationship between Southern Ocean SST (vertical axis, change since LGM), CO<sub>2</sub> (horizontal  
686 axis) and AMOC strength anomaly from the mean strength between 20–11 ka (colours). The trajectory  
687 of the deglacial CO<sub>2</sub> forcing (CO<sub>2</sub>), simulated SST changes and AMOC are plotted with circles at 200-  
688 year intervals. Note that the vertical axes are different between models to represent the total deglacial  
689 warming.



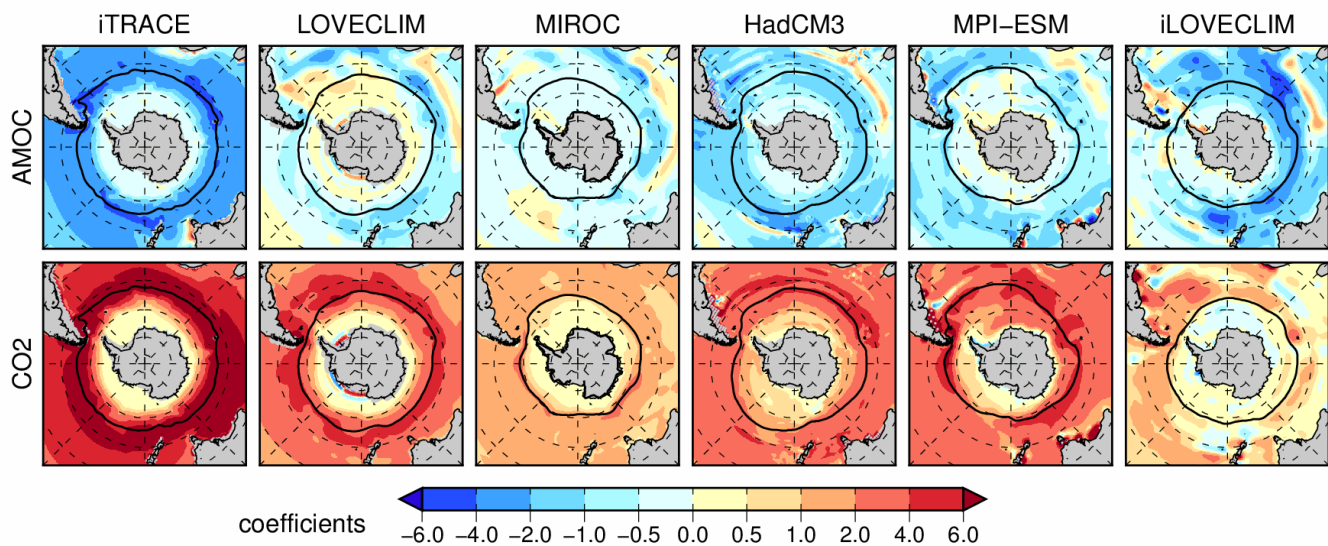


**Figure 8:** Results of the MLR model for 2-D SST maps. Top and bottom panels indicate AMOC [K/normalised AMOC] and CO<sub>2</sub> coefficients [K/83 ppm]. The black lines represent LGM winter sea ice edges.

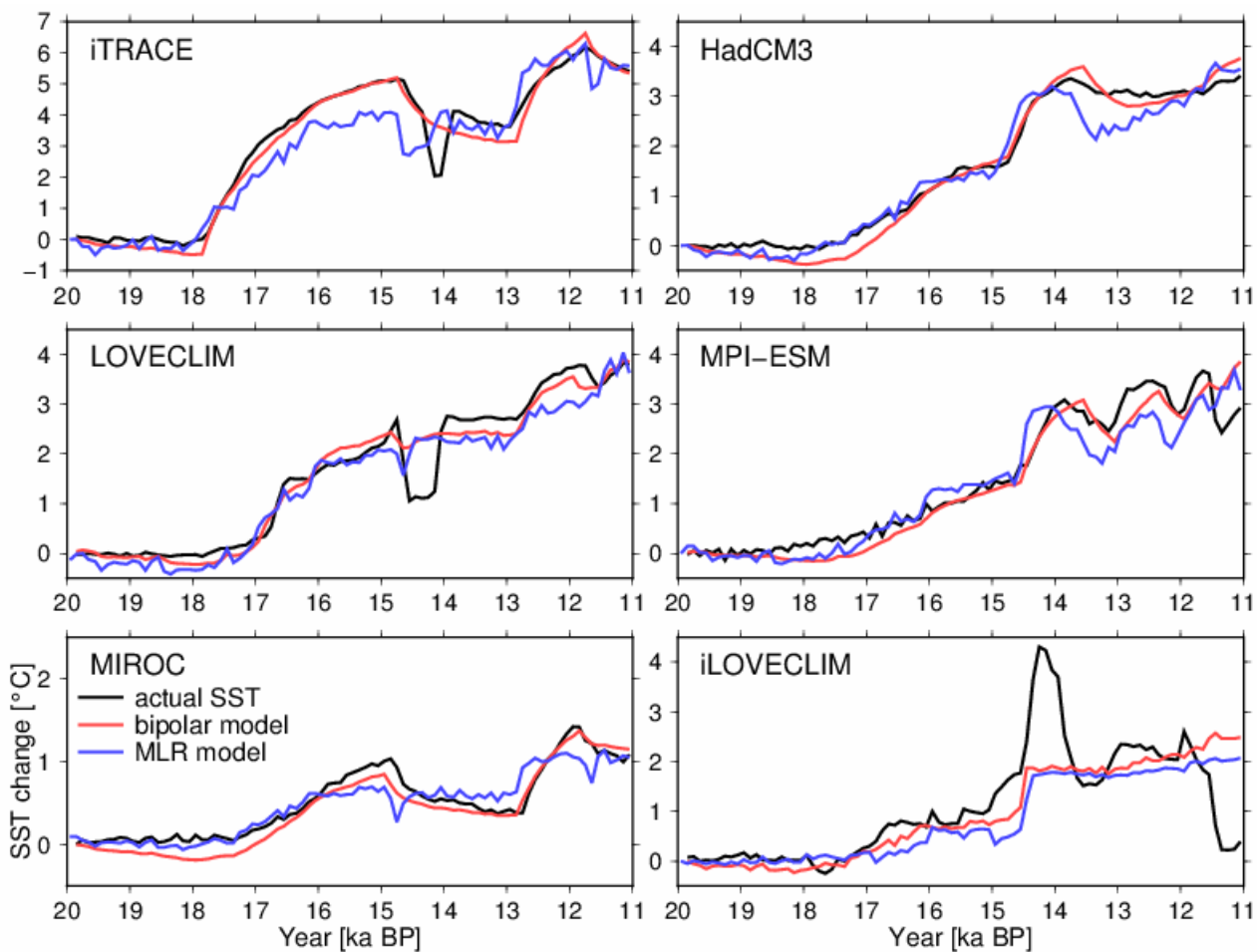


**Figure 9:** Results of the MLR model and bipolar seesaw model for Southern Ocean SST. The black lines represent the actual SST change (anomaly from 20 ka). The blue and red lines represent the results of MLR and bipolar seesaw models, respectively.

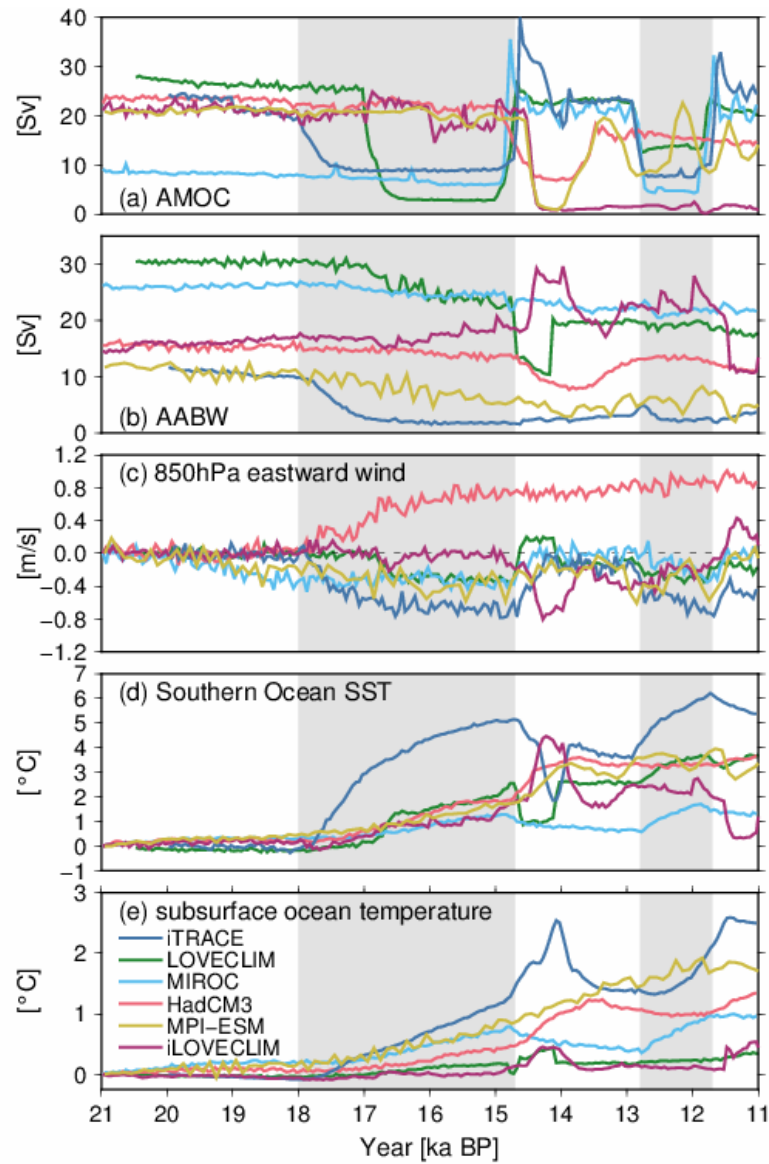


**Figure 10:** Time series of simulated (a) AMOC, (b) Antarctic Bottom Water, (c) 850 hPa eastward winds over the Southern Ocean (65–40°S), (d) Southern Ocean SST, and (e) subsurface ocean temperature south of 60°S (at depths 400–666m). The vertical grey shading indicates Heinrich Stadial 1 (18–14.7 ka) and the Younger Dryas (12.8–11.7 ka), respectively, and the period in between corresponds to the Bølling-Allerød (14.7–12.8 ka).

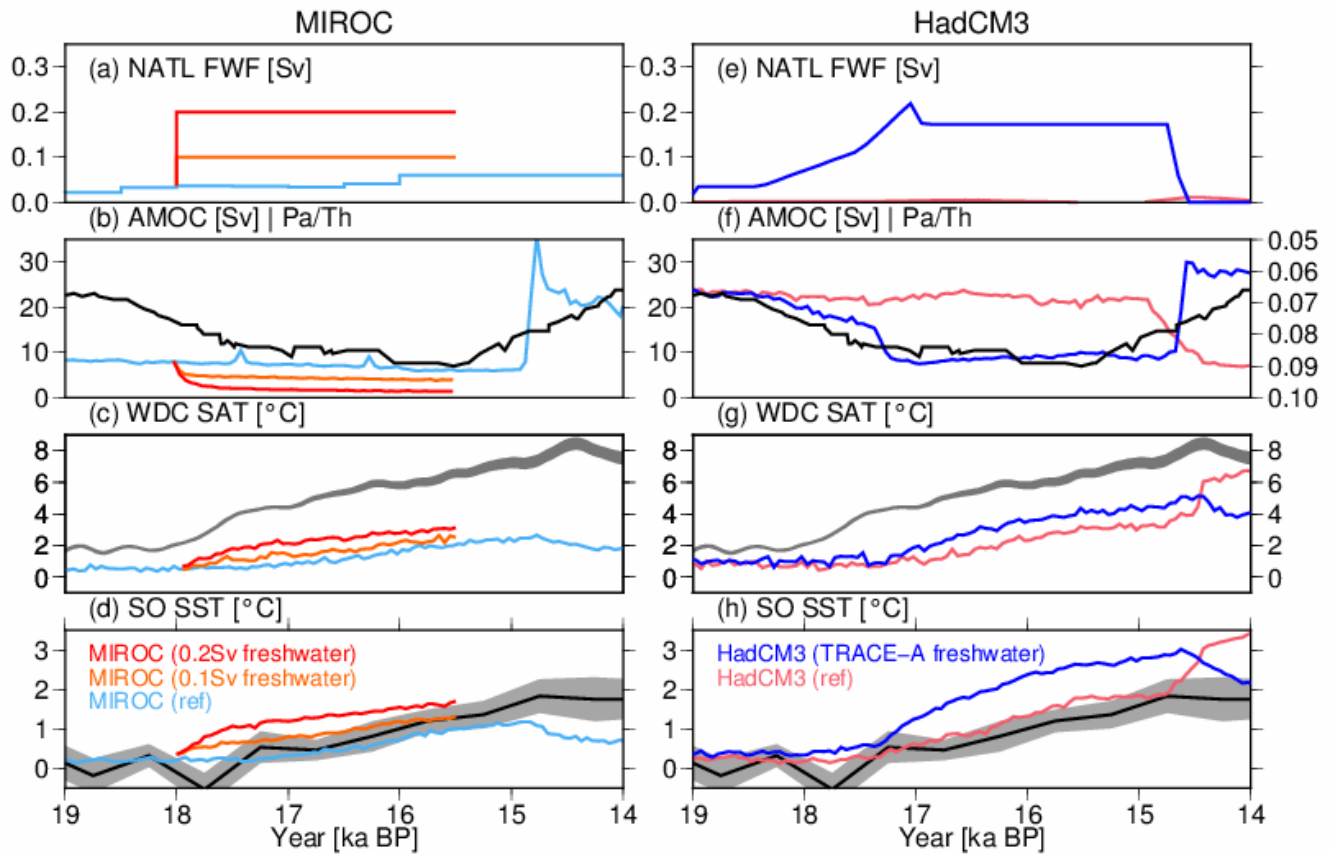


**Figure 11:** Results from transient deglaciation experiments performed with (left) MIROC and (right) HadCM3. The black lines in each panel represent the same proxy data as in Figure 3 (Parrenin et al., 2013; Buizert et al., 2021; Anderson et al., 2020). In two MIROC sensitivity experiments, a larger amount of freshwater flux (0.1 or 0.2 Sv) is added into the North Atlantic (50–70°N) during 18–15.5 ka compared to the standard MIROC experiment (light blue lines). In the TRACE-A HadCM3 sensitivity experiment (blue lines), a larger freshwater flux is added in the North Atlantic following the Trace-21ka simulation (Liu et al., 2009), while the pink lines in (b) represent the HadCM3 simulation used by Snoll et al. (2022).

## References

1. Abe-Ouchi, A., Saito, F., Kawamura, K., Raymo, M. E., Okuno, J., Takahashi, K., and Blatter, H.: Insolation-driven 100,000-year glacial cycles and hysteresis of ice-sheet volume. *Nature* 500, 190–193, doi: 10.1038/nature12374, 2013

2. Abe-Ouchi, A., Saito, F., Kageyama, M., Braconnot, P., Harrison, S. P., Lambeck, K., Otto-Bliesner, B. L., Peltier, W. R., Tarasov, L., Peterschmitt, J.-Y., and Takahashi, K.: Ice-sheet configuration in the CMIP5/PMIP3 Last Glacial Maximum experiments, *Geosci. Model Dev.*, 8, 3621–3637, doi:10.5194/gmd-8-3621-2015, 2015.
3. Anderson, B. E., & Burckle, L. H.: Rise in Atmospheric CO<sub>2</sub>. *Science*, 323 (March), 1443–1448, 2009
4. Anderson, H. J., Pedro, J. B., Bostock, H. C., Chase, Z., and Noble, T. L.: Compiled Southern Ocean sea surface temperatures correlate with Antarctic Isotope Maxima, *Quaternary Science Reviews*, 255, 106821, <https://doi.org/10.1016/j.quascirev.2021.106821>, 2021.
5. Anderson, Harris J; Pedro, Joel B; Bostock, Helen C; Chase, Zanna; Noble, Taryn L (2020): Southern Ocean Sea Surface Temperature Anomaly Stacks [dataset]. PANGAEA, <https://doi.org/10.1594/PANGAEA.912158>
6. Annan, J. D., Hargreaves, J. C., and Mauritsen, T.: A new global surface temperature reconstruction for the Last Glacial Maximum, *Clim. Past*, 18, 1883–1896, <https://doi.org/10.5194/cp-18-1883-2022>, 2022.
7. Bentley, M. J., Ocofaigh, C., Anderson, J. B., Conway, H., Davies, B., Graham, A. G. C., Hillenbrand, C. D., Hodgson, D. A., Jamieson, S. S. R., Larter, R. D., Mackintosh, A., Smith, J. A., Verleyen, E., Ackert, R. P., Bart, P. J., Berg, S., Brunstein, D., Canals, M., Colhoun, E. A., Crosta, X., Dickens, W. A., Domack, E., Dowdeswell, J. A., Dunbar, R., Ehrmann, W., Evans, J., Favier, V., Fink, D., Fogwill, C. J., Glasser, N. F., Gohl, K., Golledge, N. R., Goodwin, I., Gore, D. B., Greenwood, S. L., Hall, B. L., Hall, K., Hedding, D. W., Hein, A. S., Hocking, E. P., Jakobsson, M., Johnson, J. S., Jomelli, V., Jones, R. S., Klages, J. P., Kristoffersen, Y., Kuhn, G., Leventer, A., Licht, K., Lilly, K., Lindow, J., Livingstone, S. J., Massé, G., McGlone, M. S., McKay, R. M., Melles, M., Miura, H., Mulvaney, R., Nel, W., Nitsche, F. O., O'Brien, P. E., Post, A. L., Roberts, S. J., Saunders, K. M., Selkirk, P. M., Simms, A. R., Spiegel, C., Stolldorf, T. D., Sugden, D. E., van der Putten, N., van Ommen, T., Verfaillie, D., Vyverman, W., Wagner, B., White, D. A., Witus, A. E., and Zwart, D.: A community-based geological reconstruction of Antarctic Ice Sheet deglaciation since the Last

- Glacial Maximum, *Quaternary Sci. Rev.*, 100, 1–9, <https://doi.org/10.1016/j.quascirev.2014.06.025>, 2014.
8. Berger, A.: Long-Term Variations of Daily Insolation and Quaternary Climatic Changes, *J. Atmos. Sci.*, 35, 2362–2367, doi:10.1175/1520-0469(1978)035<2362:LTVODI>2.0.CO;2, 1978.
  9. Bereiter, B., Eggleston, S., Schmitt, J., Nehrbass-Ahles, C., Stocker, T. F., Fischer, H., Kipfstuhl, S., and Chappellaz, J.: Revision of the EPICA Dome C CO<sub>2</sub> record from 800 to 600 kyr before present, *Geophys. Res. Lett.*, 42, 542–549, 10.1002/2014GL061957, 2015.
  10. Bereiter, B., Shackleton, S., Baggenstos, D., Kawamura, K., and Severinghaus, J.: Mean global ocean temperatures during the last glacial transition. *Nature*, 553(7686), 39–44. <https://doi.org/10.1038/nature25152>, 2018.
  11. Bethke, I., Li, C., and Nisancioglu, K. H.: Can we use ice sheet reconstructions to constrain meltwater for deglacial simulations? *Paleoceanography*, 27 (November 2011), 1–17. doi:10.1029/2011PA002258, 2012
  12. Böhm, E., Lippold, J., Gutjahr, M., Frank, M., Blaser, P., Antz, B., Fohlmeister, J., Frank, N., Andersen, M. B. and Deininger, M.: Strong and deep Atlantic meridional overturning circulation during the last glacial cycle. *Nature*, 517(7534), 73–76. <https://doi.org/10.1038/nature14059>, 2015.
  13. Bouttes, N., Roche, D. M., and Paillard, D.: Systematic study of the impact of fresh water fluxes on the glacial carbon cycle, *Clim. Past*, 8, 589–607, <https://doi.org/10.5194/cp-8-589-2012>, 2012.
  14. Bouttes, N., Lhardy, F., Quiquet, A., Paillard, D., Goosse, H., and Roche, D. M.: Deglacial climate changes as forced by different ice sheet reconstructions, *Clim. Past*, 19, 1027–1042, <https://doi.org/10.5194/cp-19-1027-2023>, 2023.
  15. Buizert, C., Gkinis, V., Severinghaus, J. P., He, F., Lecavalier, B. S., Kindler, P., Leuenberger, M., Carlson, A. E., Vinther, B., Masson-Delmotte, V., White, J. W. C., Liu, Z., Otto-Bliesner, B., and Brook, E. J.: Greenland temperature response to climate forcing during the last deglaciation, *Science*, 345, 1177–1180, 10.1126/science.1254961, 2014.
  16. Buizert, C., Fudge, T. J., Roberts, W. H., Steig, E. J., Sherriff-Tadano, S., Ritz, C., Lefebvre, E., Edwards, J., Kawamura, K., Oyabu, I., Motoyama, H., Kahle, E. C., Jones, T. R., Abe-ouchi, A., Obase, T., Martin, C., Corr, H., Severinghaus, J. P., Beaudette, R., Epifanio, J. A., Brook, E. J., Martin,

- K., Aoki, S., Nakazawa, T., Sowers, T. A., Alley, R. B., Ahn, J., Sigl, M., Severi, M., Dunbar, N. W., Svensson, A., Fegyveresi, J. M., He, C., Liu, Z., Zhu, J., Otto-bliesner, B. L., Lipenkov, V. Y., Kageyama, M., and Schwander, J.: Antarctic surface temperature and elevation during the Last Glacial Maximum, *Science* 372(6546), 1097-1101, doi: 10.1126/science.abd2897, 2021
17. Burke, A. and Robinson, L. F.: The Southern Ocean's Role in Carbon Exchange During the Last Deglaciation, *Science*, 135, 6068, 557-561. <https://doi.org/10.1126/science.1208163>, 2011
18. Capron, E., Landais, A., Chappellaz, J., Schilt, A., Buiron, D., Dahl-Jensen, D., Johnsen, S. J., Jouzel, J., Lemieux-Dudon, B., Loulergue, L., Leuenberger, M., Masson-Delmotte, V., Meyer, H., Oerter, H., and Stenni, B.: Millennial and sub-millennial scale climatic variations recorded in polar ice cores over the last glacial period, *Clim. Past*, 6, 345–365, <https://doi.org/10.5194/cp-6-345-2010>, 2010.
19. Chan, W.-L. and Abe-Ouchi, A.: Pliocene Model Intercomparison Project (PlioMIP2) simulations using the Model for Interdisciplinary Research on Climate (MIROC4m), *Clim. Past*, 16, 1523–1545, <https://doi.org/10.5194/cp-16-1523-2020>, 2020.
20. Clark, P. U., He, F., Golledge, N. R., Mitrovica, J. X., Dutton, A., Hoffman, J. S., and Dendy, S.: Oceanic forcing of penultimate deglacial and last interglacial sea-level rise. *Nature*, 577(7792), 660–664. <https://doi.org/10.1038/s41586-020-1931-7>, 2020
21. Condron, A., & Winsor, P.: Meltwater routing and the Younger Dryas. *Proceedings of the National Academy of Sciences*, 109(49), 19928–19933, <https://doi.org/10.1073/pnas.1207381109>, 2012
22. Crosta, X., Kohfeld, K. E., Bostock, H. C., Chadwick, M., Du Vivier, A., Esper, O., Etourneau, J., Jones, J., Leventer, A., Müller, J., Rhodes, R. H., Allen, C. S., Ghadi, P., Lamping, N., Lange, C. B., Lawler, K.-A., Lund, D., Marzocchi, A., Meissner, K. J., Menviel, L., Nair, A., Patterson, M., Pike, J., Prebble, J. G., Riesselman, C., Sadatzki, H., Sime, L. C., Shukla, S. K., Thöle, L., Vorrath, M.-E., Xiao, W., and Yang, J.: Antarctic sea ice over the past 130 000 years – Part 1: a review of what proxy records tell us, *Clim. Past*, 18, 1729–1756, <https://doi.org/10.5194/cp-18-1729-2022>, 2022.
23. Dansgaard, W., Johnsen, S. J., Clausen, H. B., Dahl-Jensen, D., Gundestrup, N. S., Hammer, C. U., Hvidberg, C. S., Steffensen, J. P., Sveinbjörnsdottir, A. E., Jouzel, J., and Bond, G.: Evidence for general instability of past climate from a 250-kyr ice-core record, *Nature*, 364, 218–220, <https://doi.org/10.1038/364218a0>, 1993

24. Deschamps, P., Durand, N., Bard, E., Hamelin, B., Camoin, G., Thomas, A. L., Henderson, G. M., Okuno, J., and Yokoyama, Y.: Ice-sheet collapse and sea-level rise at the Bølling warming 14,600 years ago, *Nature*, 28, 559–564, <https://doi.org/10.1038/nature10902>, 2012.
25. Ferrari, R., Jansen, M. F., Adkins, J. F., Burke, A., Stewart, A. L., and Thompson, A. F.: Antarctic sea ice control on ocean circulation in present and glacial climates, *P. Natl. Acad. Sci. USA*, 111, 8753–8758, [10.1073/pnas.1323922111](https://doi.org/10.1073/pnas.1323922111), 2014.
26. Golledge, N., Menviel, L., Carter, L., Fogwill, C. J., England, M. H., Cortese, G., and Levy, R. H.: Antarctic contribution to meltwater pulse 1A from reduced Southern Ocean overturning. *Nat Commun* 5, 5107, <https://doi.org/10.1038/ncomms6107>, 2014.
27. Gomez, N., Weber, M. E., Clark, P. U., Mitrovica, J. X. and Han, H. K.: Antarctic ice dynamics amplified by Northern Hemisphere sea-level forcing, *Nature*, 587(7835), 600–604, [doi:10.1038/s41586-020-2916-2](https://doi.org/10.1038/s41586-020-2916-2), 2020
28. Goosse, H., Brovkin, V., Fichefet, T., Haarsma, R., Huybrechts, P., Jongma, J., Mouchet, A., Selten, F., Barriat, P.-Y., Campin, J.-M., Deleersnijder, E., Driesschaert, E., Goelzer, H., Janssens, I., Loutre, M.-F., Morales Maqueda, M. A., Opsteegh, T., Mathieu, P.-P., Munhoven, G., Pettersson, E. J., Renssen, H., Roche, D. M., Schaeffer, M., Tartinville, B., Timmermann, A., and Weber, S. L.: Description of the Earth system model of intermediate complexity LOVECLIM version 1.2, *Geosci. Model Dev.*, 3, 603–633, <https://doi.org/10.5194/gmd-3-603-2010>, 2010.
29. Gottschalk, J., Battaglia, G., Fischer, H., Frölicher, T. L., Jaccard, S. L., Jeltsch-Thömmes, A., Joos, F., Köhler, P., Meissner, K. J., Menviel, L., Nehrbass-Ahles, C., Schmitt, J., Schmittner, A., Skinner, L. C., and Stocker, T. F.: Mechanisms of millennial-scale atmospheric CO<sub>2</sub> change in numerical model simulations, *Quaternary Sci. Rev.*, 220, 30–74, <https://doi.org/10.1016/j.quascirev.2019.05.013>, 2019.
30. Gray, W. R., de Lavergne, C., Willis, R. C. J., Menviel, L., Spence, P., Holzer, M., Kageyama, M. and Michel, E.: Poleward Shift in the Southern Hemisphere Westerly Winds Synchronous With the Deglacial Rise in CO<sub>2</sub>, *Paleoceanography and Paleoclimatology*, 38, 7, <https://doi.org/10.1029/2023PA004666>, 2023



- 829 31. Green, R. A., Menviel, L., Meissner, K. J., Crosta, X., Chandan, D., Lohmann, G., Peltier, W. R., Shi,  
830 X., and Zhu, J.: Evaluating seasonal sea-ice cover over the Southern Ocean at the Last Glacial  
831 Maximum, *Clim. Past*, 18, 845–862, <https://doi.org/10.5194/cp-18-845-2022>, 2022.
- 832 32. Gregoire, L. J., Payne, A. J., and Valdes, P. J.: Deglacial rapid sea level rises caused by ice-sheet  
833 saddle collapses, *Nature*, 487, 219–222, 10.1038/nature11257, 2012.
- 834 33. He, F., Shakun, J. D., Clark, P. U., Carlson, A. E., Liu, Z., Otto-Bliesner, B. L., and Kutzbach, J. E.:  
835 Northern Hemisphere forcing of Southern Hemisphere climate during the last deglaciation, *Nature*,  
836 494, 81–85, <https://doi.org/10.1038/nature11822>, 2013.
- 837 34. He, C., Zhengyu Liu, and Aixue Hu.: The transient response of atmospheric and oceanic heat  
838 transports to anthropogenic warming. *Nature Climate Change*, 1, doi:10.1038/s41558-018-0387-3,  
839 2019.
- 840 35. He, C., Liu, Z., Zhu, J., Zhang, J., Gu, S., Otto-Bliesner, B. L., Brady, E., Zhu, C., Jin, Y. and Sun,  
841 J.: North Atlantic subsurface temperature response controlled by effective freshwater input in  
842 “Heinrich” events, *Earth and Planetary Science Letters*, 539, 116247,  
843 <https://doi.org/10.1016/j.epsl.2020.116247>, 2020.
- 844 36. He, C., Liu, Z., Otto-Bliesner, B. L., Brady, E. C., Zhu, C., Tomas, R., Bao, Y.: Hydroclimate  
845 footprint of pan-Asian monsoon water isotope during the last deglaciation. *Science Advances*, 7(4),  
846 1–12. <https://doi.org/10.1126/sciadv.abe2611>, 2021.
- 847 37. Hunter, S. J., Haywood, A. M., Dolan, A. M., and Tindall, J. C.: The HadCM3 contribution to  
848 PlioMIP phase 2, *Clim. Past*, 15, 1691–1713, <https://doi.org/10.5194/cp-15-1691-2019>, 2019.
- 849 38. Ivanovic, R. F., Gregoire, L. J., Kageyama, M., Roche, D. M., Valdes, P. J., Burke, A., Drummond,  
850 R., Peltier, W. R., and Tarasov, L.: Transient climate simulations of the deglaciation 21–9 thousand  
851 years before present (version 1) – PMIP4 Core experiment design and boundary conditions, *Geosci.*  
852 *Model Dev.*, 9, 2563–2587, <https://doi.org/10.5194/gmd-9-2563-2016>, 2016.
- 853 39. Ivanovic, R. F., Gregoire, L. J., Burke, A., Wickert, A. D., and Valdes, P. J.: Acceleration of Northern  
854 Ice Sheet Melt Induces AMOC Slowdown and Northern Cooling in Simulations of the Early Last  
855 Deglaciation, *Paleoceanography and Paleoclimatology*. 807–824. doi:10.1029/2017PA003308, 2018

- 856 40. Jouzel, J., Masson-Delmotte, V., Cattani, O., Dreyfus, G., Falourd, S., Hoffmann, G., Minster, B.,  
857 Nouet, J., Barnola, J. M., Chappellaz, J., Fischer, H., Gallet, J. C., Johnsen, S., Leuen-  
858 Louergue, L., Luethi, D., Oerter, H., Parrenin, F., Raisbeck, G., Raynaud, D., Schilt, A., Schwander,  
859 J., Selmo, E., Souchez, R., Spahni, R., Stauffer, B., Steffensen, J. P., Stenni, B., Stocker, T. F., Tison,  
860 J. L., Werner, M., and Wolff, E. W.: Orbital and Millennial Antarctic Climate Variability over the  
861 Past 800,000 Years, *Science*, 317, 793-796, <https://doi.org/10.1126/science.1141038>, 2007.
- 862 41. Kageyama, M., Merkel, U., Otto-Bliesner, B., Prange, M., Abe-Ouchi, A., Lohmann, G., Ohgaito,  
863 R., Roche, D. M., Singarayer, J., Swingedouw, D., and X Zhang: Climatic impacts of fresh water  
864 hosing under Last Glacial Maximum conditions: a multi-model study, *Clim. Past*, 9, 935–953,  
865 <https://doi.org/10.5194/cp-9-935-2013>, 2013.
- 866 42. Kageyama, M., Braconnot, P., Harrison, S. P., Haywood, A. M., Jungclaus, J. H., Otto-Bliesner, B.  
867 L., Peterschmitt, J.-Y., Abe-Ouchi, A., Albani, S., Bartlein, P. J., Brierley, C., Crucifix, M., Dolan,  
868 A., Fernandez-Donado, L., Fischer, H., Hopcroft, P. O., Ivanovic, R. F., Lambert, F., Lunt, D. J.,  
869 Mahowald, N. M., Peltier, W. R., Phipps, S. J., Roche, D. M., Schmidt, G. A., Tarasov, L., Valdes,  
870 P. J., Zhang, Q., and Zhou, T.: The PMIP4 contribution to CMIP6 – Part 1: Overview and over-  
871 arching analysis plan, *Geosci. Model Dev.*, 11, 1033–1057, [https://doi.org/10.5194/gmd-11-1033-](https://doi.org/10.5194/gmd-11-1033-2018)  
872 2018, 2018.
- 873 43. Kageyama, M., Harrison, S. P., Kapsch, M.-L., Lofverstrom, M., Lora, J. M., Mikolajewicz, U.,  
874 Sherriff-Tadano, S., Vadsaria, T., Abe-Ouchi, A., Bouttes, N., Chandan, D., Gregoire, L. J., Ivanovic,  
875 R. F., Izumi, K., LeGrande, A. N., Lhardy, F., Lohmann, G., Morozova, P. A., Ohgaito, R., Paul, A.,  
876 Peltier, W. R., Poulsen, C. J., Quiquet, A., Roche, D. M., Shi, X., Tierney, J. E., Valdes, P. J., Volodin,  
877 E., and Zhu, J.: The PMIP4 Last Glacial Maximum experiments: preliminary results and comparison  
878 with the PMIP3 simulations, *Clim. Past*, 17, 1065–1089, <https://doi.org/10.5194/cp-17-1065-2021>,  
879 2021.
- 880 44. Kapsch, M.-L., Mikolajewicz, U., Ziemen, F. and Schannwell, C.: Ocean response in transient  
881 simulations of the last deglaciation dominated by underlying ice-sheet reconstruction and method of  
882 meltwater distribution, *Geophysical Research Letters*, 49, e2021GL096767,  
883 <https://doi.org/10.1029/2021GL096767>, 2022.

- 884 45. Kobayashi, H., Oka, A., Yamamoto, A., and Abe-Ouchi, A.: Glacial carbon cycle changes by  
885 Southern Ocean processes with sedimentary amplification. *Science Advances*, 7(35), doi:  
886 10.1126/sciadv.abg7723, 2021.
- 887 46. Kobayashi, H., Oka, A., Obase, T., and Abe-Ouchi, A.: Assessing transient changes in the ocean  
888 carbon cycle during the last deglaciation through carbon isotope modeling, *Clim. Past*, 20, 769–787,  
889 <https://doi.org/10.5194/cp-20-769-2024>, 2024.
- 890 47. Kuniyoshi, Y., Abe-Ouchi, A., Sherriff-Tadano, S., Chan, W.-L., and Saito, F.: Effect of Climatic  
891 Precession on Dansgaard-Oeschger-Like Oscillations. *Geophysical Research Letters*, 49(6),  
892 e2021GL095695. <https://doi.org/10.1029/2021GL095695>, 2022.
- 893 48. Lambeck, K., Rouby, H., Purcell, A., Sun, Y., and Sambridge, M.: Sea level and global ice volumes  
894 from the Last Glacial Maximum to the Holocene, *P. Natl. Acad. Sci.*, 111, 15296–15303,  
895 10.1073/pnas.1411762111, 2014.
- 896 49. Lhardy, F., Bouttes, N., Roche, D. M., Crosta, X., Waelbroeck, C., and Paillard, D.: Impact of  
897 Southern Ocean surface conditions on deep ocean circulation during the LGM: a model analysis,  
898 *Clim. Past*, 17, 1139–1159, <https://doi.org/10.5194/cp-17-1139-2021>, 2021.
- 899 50. Lisiecki, L. E. and Raymo, M. E.: A Pliocene-Pleistocene stack of 57 globally distributed benthic  
900  $\delta^{18}\text{O}$  records, *Paleoceanography*, 20, PA1003, doi:10.1029/2004PA001071, 2005
- 901 51. Liu, Z., Otto-Bliesner, B. L., He, F., Brady, E. C., Tomas, R., Clark, P. U., Carlson, A. E., Lynch-  
902 Stieglitz, J., Curry, W., Brook, E., Erickson, D., Jacob, R., Kutzbach, J., and Cheng, J.: Transient  
903 Simulation of Last Deglaciation with a New Mechanism for Bølling-Allerød Warming, *Science*, 325,  
904 310–314, doi:10.1126/science.1171041, 2009
- 905 52. Liu, Z., Bao, Y., Thompson, L. G., Mosley-Thompson, E., Tabor, C., Zhang, G. J., Yan, M.,  
906 Lofverstrom, M., Montanez, I., and Oster, J.: Tropical mountain ice core  $\delta^{18}\text{O}$ : A Goldilocks  
907 indicator for global temperature change, *Science Advances*, 9, 45,  
908 <https://doi.org/10.1126/sciadv.adi6725>, 2023
- 909 53. Love, R., Andres, H. J., Condron, A., and Tarasov, L.: Freshwater routing in eddy-permitting  
910 simulations of the last deglacial: the impact of realistic freshwater discharge, *Clim. Past*, 17, 2327–  
911 2341, <https://doi.org/10.5194/cp-17-2327-2021>, 2021.

- 912 54. Lowry, D. P., Golledge, N. R., Menviel, L., and Bertler, N. A. N.: Deglacial evolution of regional  
913 Antarctic climate and Southern Ocean conditions in transient climate simulations. 189–215, 2018.
- 914 55. Lynch-Stieglitz, J., Adkins, J. F., Curry, W. B., Dokken, T., Hall, I. R., Herguera, J. C. and Zahn, R.:  
915 Atlantic meridional overturning circulation during the Last Glacial Maximum. *Science*, 316(5821),  
916 66–69. <https://doi.org/10.1126/science.1137127>, 2007
- 917 56. MacDougall, A. H., Frölicher, T. L., Jones, C. D., Rogelj, J., Matthews, H. D., Zickfeld, K., Arora,  
918 V. K., Barrett, N. J., Brovkin, V., Burger, F. A., Eby, M., Eliseev, A. V., Hajima, T., Holden, P. B.,  
919 Jeltsch-Thömmes, A., Koven, C., Mengis, N., Menviel, L., Michou, M., Mokhov, I. I., Oka, A.,  
920 Schwinger, J., Séférian, R., Shaffer, G., Sokolov, A., Tachiiri, K., Tjiputra, J., Wiltshire, A., and  
921 Ziehn, T.: Is there warming in the pipeline? A multi-model analysis of the Zero Emissions  
922 Commitment from CO<sub>2</sub>, *Biogeosciences*, 17, 2987–3016, <https://doi.org/10.5194/bg-17-2987-2020>,  
923 2020.
- 924 57. Marcott, S. A., Bauska, T. K., Buizert, C., Steig, E. J., Rosen, J. L., Cuffey, K. M., Fudge, T. J.,  
925 Severinghaus, J. P., Kalk, M. L., McConnell, J. R., Sowers, T., Taylor, K. C. White, J. W. C. and  
926 Brook, E. J.: Centennial-scale changes in the global carbon cycle during the last deglaciation. *Nature*,  
927 514(7524), 616–619. <https://doi.org/10.1038/nature13799>, 2014
- 928 58. Margari, V., Skinner, L. C., Menviel, L., Capron, E., Rhodes, R. H., Martrat, B., and Grimalt, J. O.:  
929 Fast and slow components of interstadial warming in the North Atlantic during the last glacial.  
930 *Communications Earth & Environment*, 1–9. <https://doi.org/10.1038/s43247-020-0006-x>, 2020
- 931 59. Mariotti, V., Paillard, D., Bopp, L., Roche, D. M., and Bouttes, N.: A coupled model for carbon and  
932 radiocarbon evolution during the last deglaciation. *Geophysical Research Letters*, 43(3), 1306–1313.  
933 <https://doi.org/10.1002/2015GL067489>, 2016.
- 934 60. Marson, J. M., Mysak, L. A., Mata, M. M., and Wainer, I.: Evolution of the deep Atlantic water  
935 masses since the last glacial maximum based on a transient run of NCAR-CCSM3. *Climate Dynamics*,  
936 47(3–4), 865–877. <https://doi.org/10.1007/s00382-015-2876-7>, 2016
- 937 61. Martínez-García, A., Rosell-Melé, A., Jaccard, S.: Southern Ocean dust–climate coupling over the  
938 past four million years. *Nature* 476, 312–315. <https://doi.org/10.1038/nature10310>, 2011.

- 939 62. Martrat, B., Grimalt, J. O., Shackleton, N. J., de Abreu, L., Hutterli, M.A., and Stocker, T. F.: Four  
940 climate cycles of recurring deep and surface water destabilizations on the Iberian Margin, *Science*,  
941 317, 502–507, doi:10.1126/science.1139994, 2007.
- 942 63. Marzocchi, A. and Jansen, M. F. Global cooling linked to increased glacial carbon storage via  
943 changes in Antarctic sea ice. *Nature Geoscience*, 12, 1001–1005, [https://doi.org/10.1038/s41561-](https://doi.org/10.1038/s41561-019-0466-8)  
944 019-0466-8, 2019
- 945 64. Masoum, A., Nerger, L., Willeit, M., Ganopolski, A., and Lohmann, G.: Lessons From Transient  
946 Simulations of the Last Deglaciation With CLIMBER-X: GLAC1D Versus PaleoMist, *Geophysical*  
947 *Research Letters*, 51(16), e2023GL107310. <https://doi.org/10.1029/2023GL107310>, 2024.
- 948 65. McManus, J. F., Francois, R., Gherardi, J.-M., Keigwin, L. D., and Brown-Leger, S.: Collapse and  
949 rapid resumption of Atlantic meridional circulation linked to deglacial climate changes, *Nature*, 428,  
950 834–837, 10.1038/nature02494, 2004.
- 951 66. Menviel, L., Yu, J., Joos, F., Mouchet, A., Meissner, K. J., and England, M. H.: Poorly ventilated  
952 deep ocean at the Last Glacial Maximum inferred from carbon isotopes: A data-model comparison  
953 study. *Paleoceanography*, 32(1), 2–17. <https://doi.org/10.1002/2016PA003024>, 2017.
- 954 67. Menviel, L., Timmermann, a., Timm, O. E., and Mouchet, A.: Climate and biogeochemical response  
955 to a rapid melting of the West Antarctic Ice sheet during interglacials and implications for future  
956 climate. *Paleoceanography*, 25, 1–12. <https://doi.org/10.1029/2009PA001892>, 2010.
- 957 68. Menviel, L., Timmermann, A., Timm, O. E., and Mouchet, A.: Deconstructing the Last Glacial  
958 termination: the role of millennial and orbital-scale forcings, *Quaternary Sci. Rev.*, 30, 1155–1172,  
959 10.1016/j.quascirev.2011.02.005, 2011.
- 960 69. Menviel, L., England, M. H., Meissner, K. J., Mouchet, A., and Yu, J.: Atlantic-Pacific seesaw and  
961 its role in outgassing CO<sub>2</sub> during Heinrich events. *Paleoceanography*, 29(January), 58–70.  
962 <https://doi.org/10.1002/2013PA002542>, 2014.
- 963 70. Menviel, L., Spence, P., Yu, J., Chamberlain, M. A., Matear, R. J., Meissner, K. J., and England, M.  
964 H.: Southern Hemisphere westerlies as a driver of the early deglacial atmospheric CO<sub>2</sub> rise. *Nature*  
965 *Communications*, 9(1), 1–12. <https://doi.org/10.1038/s41467-018-04876-4>, 2018

- 966 71. Moros, M., De Deckker, P., Perner, K., Ninnemann, U. S., Wacker, L., Telford, R., Jansen, E., Blanz,  
967 T. and Schneider, R.: Hydrographic shifts south of Australia over the last deglaciation and possible  
968 interhemispheric linkages. *Quaternary Research (United States)*, 102, 130–141.  
969 <https://doi.org/10.1017/qua.2021.12>, 2021
- 970 72. Morrison, A. and Hogg, A.: On the Relationship between Southern Ocean Overturning and ACC  
971 Transport, *J. Phys. Oceanogr.*, 43, 140–148, 2013.
- 972 73. Moy, A. D., Palmer, M. R., Howard, W. R., Bijma, J., Cooper, M. J., Calvo, E., Pelejero, C., Gagan,  
973 M. K. and Chalk, T. B.: Varied contribution of the Southern Ocean to deglacial atmospheric CO<sub>2</sub>  
974 rise. *Nature Geoscience*, 12(12), 1006–1011. <https://doi.org/10.1038/s41561-019-0473-9>, 2019
- 975 74. Ng, H. C., Robinson, L. F., McManus, J. F., Mohamed, K. J., Jacobel, A. W., Ivanovic, R. F.,  
976 Gregoire, L. J. and Chen, T.: Coherent deglacial changes in western Atlantic Ocean circulation.  
977 *Nature Communications*, 9(1), 1–10. <https://doi.org/10.1038/s41467-018-05312-3>, 2018
- 978 75. Obase, T., and Abe- Ouchi, A.: Abrupt Bølling-Allerød warming simulated under gradual forcing of  
979 the last deglaciation, *Geophysical Research Letters*, 46, <https://doi.org/10.1029/2019GL084675>,  
980 2019.
- 981 76. Obase, T., A. Abe-Ouchi, F. Saito: Abrupt climate changes in the last two deglaciations simulated  
982 with different Northern ice sheet discharge and insolation, *Scientific Reports*, 11, doi:  
983 10.1038/s41598-021-01651-2, 2021
- 984 77. Parrenin, F., Masson-Delmotte, V., Köhler, P., Raynaud, D., Paillard, D., Schwander, J., Barbante,  
985 C., Landais, A., Wegner, A., Jouzel, J.: Atmospheric carbon dioxide, methane, deuterium, and  
986 calculated Antarctic temperature of EPICA Dome C ice core. *PANGAEA*,  
987 doi:10.1594/PANGAEA.810199, 2013
- 988 78. Pedro, J. B., Martin, T., Steig, E. J., Jochum, M., Park, W., & Rasmussen, S. O.: Southern Ocean  
989 deep convection as a driver of Antarctic warming events. *Geophysical Research Letters*, 43(5), 2192–  
990 2199. <https://doi.org/10.1002/2016GL067861>, 2016
- 991 79. Pedro, J. B., Jochum, M., Buizert, C., He, F., Barker, S., & Rasmussen, S. O.: Beyond the bipolar  
992 seesaw: Toward a process understanding of interhemispheric coupling. *Quaternary Science Reviews*,  
993 192, 27–46. <https://doi.org/10.1016/j.quascirev.2018.05.005>, 2018

- 994 80. Peltier, W. R., Argus, D. F., and Drummond, R.: Space geodesy constrains ice age terminal  
 995 deglaciation: The global ICE-6G\_C (VM5a) model, *J. Geophys. Res.-Sol. Ea.*, 120, 450–487,  
 996 10.1002/2014JB011176, 2015.
- 997 81. Petit, J. R., Jouzel, J., Raynaud, D., Barkov, N. I., Barnola, J.-M., Basile, I., Bender, M., Chappellaz,  
 998 J., Davis, M., Delaygue, G., Delmotte, M., Kotlyakov, V. M., Legrand, M., Lipenkov, V. Y., Lorius,  
 999 C., PÉpin, L., Ritz, C., Saltzman, E., and Stievenard, M.: Climate and atmospheric history of the past  
 1000 420 000 years from the Vostok ice core, Antarctica, *Nature*, 399, 429–436, 10.1038/20859, 1999.
- 1001 82. Pöppelmeier, F., Jeltsch-Thömmes, A., Lippold, J. et al. Multi-proxy constraints on Atlantic  
 1002 circulation dynamics since the last ice age. *Nat. Geosci.* 16, 349–356 (2023).  
 1003 <https://doi.org/10.1038/s41561-023-01140-3>
- 1004 83. Prange, M., Jonkers, L., Merkel, U., Schulz, M. and Bakker, P: A multicentennial mode of North  
 1005 Atlantic climate variability throughout the Last Glacial Maximum, *Science*, 9, 44,  
 1006 <https://www.science.org/doi/10.1126/sciadv.adh1106>, 2023.
- 1007 84. Rae, J. W. B., Burke, A., Robinson, L. F., Adkins, J. F., Chen, T., Cole, C., Greenop, R., Li, T.,  
 1008 Littley, E. F. M., Nita, D. C., Stewart, J. A. and Taylor, B. J.: CO<sub>2</sub> storage and release in the deep  
 1009 Southern Ocean on millennial to centennial timescales, *Nature*, 562, 569–573,  
 1010 <https://doi.org/10.1038/s41586-018-0614-0>, 2018
- 1011 85. Renssen, H., Mairesse, A., Goosse, H., Mathiot, P., Heiri, O., Roche, D. M., Nisancioglu, K. H. and  
 1012 Valdes, P. J.: Multiple causes of the Younger Dryas cold period. *Nature Geoscience*, 8(12), 946–949.  
 1013 <https://doi.org/10.1038/ngeo2557>, 2015
- 1014 86. Roberts, N. L., Piotrowski, A. M., McManus, J. F., and Keigwin, L. D.: Synchronous Deglacial  
 1015 Overturning and Water Mass Source Changes, *Science*, 327, 75–78, 10.1126/science.1178068, 2010.
- 1016 87. Roche, D. M., Renssen, H., Paillard, D., & Levavasseur, G.: Deciphering the spatio-temporal  
 1017 complexity of climate change of the last deglaciation: A model analysis. *Climate of the Past*, 7(2),  
 1018 591–602. <https://doi.org/10.5194/cp-7-591-2011>, 2011
- 1019 88. Roche, D.M., Wiersma, A.P. & Renssen, H. A systematic study of the impact of freshwater pulses  
 1020 with respect to different geographical locations. *Clim Dyn* 34, 997–1013.  
 1021 <https://doi.org/10.1007/s00382-009-0578-8>, 2010.

- 1022 89. Rojas, M., Moreno, P., Kageyama, M., Crucifix, M., Hewitt, C., Abe-Ouchi, A., Ohgaito, R., Brady  
1023 E. C. and Hope, P.: The Southern Westerlies during the last glacial maximum in PMIP2 simulations.  
1024 *Climate Dynamics*, 32(4), 525–548. <https://doi.org/10.1007/s00382-008-0421-7>, 2009
- 1025 90. Sadatzki, H., Opdyke, B., Menviel, L., Leventer, A., Hope, J. M., Brocks, J. J., Fallon, S., Post, A.  
1026 L., O’Brien, P. E., Grant, K., & Armand, L.: Early sea ice decline off East Antarctica at the last  
1027 glacial-interglacial climate transition, *Science Advances*, 9, 41, doi: 10.1126/sciadv.adh9513, 2023.
- 1028 91. Schloesser, F., Friedrich, T., Timmermann, A., DeConto, R. M., and Pollard, D.: Antarctic iceberg  
1029 impacts on future Southern Hemisphere climate, *Nat. Clim. Change*, 9, 672–677,  
1030 <https://doi.org/10.1038/s41558-019-0546-1>, 2019.
- 1031 92. Seroussi, H., Nowicki, S., Payne, A. J., Goelzer, H., Lipscomb, W. H., Abe-Ouchi, A., Agosta, C.,  
1032 Albrecht, T., Asay-Davis, X., Barthel, A., Calov, R., Cullather, R., Dumas, C., Galton-Fenzi, B. K.,  
1033 Gladstone, R., Golledge, N. R., Gregory, J. M., Greve, R., Hattermann, T., Hoffman, M. J., Humbert,  
1034 A., Huybrechts, P., Jourdain, N. C., Kleiner, T., Larour, E., Leguy, G. R., Lowry, D. P., Little, C. M.,  
1035 Morlighem, M., Pattyn, F., Pelle, T., Price, S. F., Quiquet, A., Reese, R., Schlegel, N.-J., Shepherd,  
1036 A., Simon, E., Smith, R. S., Straneo, F., Sun, S., Trusel, L. D., Van Breedam, J., van de Wal, R. S.  
1037 W., Winkelmann, R., Zhao, C., Zhang, T., and Zwinger, T.: ISMIP6 Antarctica: a multi-model  
1038 ensemble of the Antarctic ice sheet evolution over the 21st century, *The Cryosphere*, 14, 3033–3070,  
1039 <https://doi.org/10.5194/tc-14-3033-2020>, 2020.
- 1040 93. Severinghaus, J. P. and Brook, E. J.: Abrupt Climate Change at the End of the Last Glacial Period  
1041 Inferred from Trapped Air in Polar Ice, *Science*, 286, 930–934, 10.1126/science.286.5441.930, 1999.
- 1042 94. Shakun, J. D., Clark, P. U., He, F., Marcott, S. A., Mix, A. C., Liu, Z., Otto-Bliesner, B., Schmittner,  
1043 A., and Bard, E.: Global warming preceded by increasing carbon dioxide concentrations during the  
1044 last deglaciation, *Nature*, 484, 49–54, 10.1038/nature10915, 2012.
- 1045 95. Sherriff-Tadano, S., Abe-Ouchi, A., Yoshimori, M., Ohgaito, R., Vadsaria, T., Chan, W.-L., Hotta,  
1046 H., Kikuchi, M., Kodama, T., Oka, A., Southern Ocean surface temperatures and cloud biases in  
1047 climate models connected to the representation of glacial deep ocean circulation, *Journal of Climate*.  
1048 3849-3866, <https://doi.org/10.1175/JCLI-D-22-0221.1>, 2023



- 1049 96. Sigman, D. M., Hain, M. P., & Haug, G. H.: The polar ocean and glacial cycles in atmospheric CO<sub>2</sub>  
1050 concentration. *Nature*, 466(7302), 47–55. <https://doi.org/10.1038/nature09149>, 2010
- 1051 97. Sikes, E. L., Schiraldi, B., & Williams, A.: Seasonal and Latitudinal Response of New Zealand Sea  
1052 Surface Temperature to Warming Climate Since the Last Glaciation: Comparing Alkenones to  
1053 Mg/Ca Foraminiferal Reconstructions. *Paleoceanography and Paleoclimatology*, 34(11), 1816–1832.  
1054 <https://doi.org/10.1029/2019PA003649>, 2019.
- 1055 98. Sime, L. C., Kohfeld, K. E., Le, C., Wolff, E. W., Boer, A. M. De, Graham, R. M., & Bopp, L.:  
1056 Southern Hemisphere westerly wind changes during the Last Glacial Maximum: model-data  
1057 comparison. *Quaternary Science Reviews*, 64, 104–120.  
1058 <https://doi.org/10.1016/j.quascirev.2012.12.008>, 2013.
- 1059 99. Skinner, L. C., Fallon, S., Waelbroeck, C., Michel, E., & Barker, S.: Ventilation of the deep Southern  
1060 Ocean and deglacial CO<sub>2</sub> rise. *Science*, 328(5982), 1147–1151.  
1061 <https://doi.org/10.1126/science.1183627>, 2010
- 1062 100. Snoll, B., Ivanovic, R.F., Valdes, P.J., Maycock, A. C. and Gregoire, L. J.: Effect of orographic  
1063 gravity wave drag on Northern Hemisphere climate in transient simulations of the last deglaciation.  
1064 *Clim Dyn* 59, 2067–2079. <https://doi.org/10.1007/s00382-022-06196-2>, 2022.
- 1065 101. Snoll, B., Ivanovic, R., Gregoire, L., Sherriff-Tadano, S., Menviel, L., Obase, T., Abe-Ouchi, A.,  
1066 Bouttes, N., He, C., He, F., Kapsch, M., Mikolajewicz, U., Muglia, J., and Valdes, P.: A multi-model  
1067 assessment of the early last deglaciation (PMIP4 LDv1): a meltwater perspective, *Clim. Past*, 20,  
1068 789–815, <https://doi.org/10.5194/cp-20-789-2024>, 2024.
- 1069 102. Steffensen, J. P., Andersen, K. K., Bigler, M., Clausen, H. B., Dahl-Jensen, D., Fischer, H., Goto-  
1070 Azuma, K., Hansson, M., Johnsen, S. J., Jouzel, J., Masson-Delmotte, V., Popp, T., Rasmussen, S.  
1071 O., Röthlisberger, R., Ruth, U., Stauffer, B., Siggaard-Andersen, M.-L., Sveinbjörnsdóttir, Á. E.,  
1072 Svensson, A., and White, J. W. C.: High-Resolution Greenland Ice Core Data Show Abrupt Climate  
1073 Change Happens in Few Years, *Science*, 321, 680–684, [10.1126/science.1157707](https://doi.org/10.1126/science.1157707), 2008.
- 1074 103. Stein, K., Timmermann, A., Young Kwon, E., and Friedrich, T.: Timing and magnitude of Southern  
1075 Ocean sea ice/carbon cycle feedbacks, *P. Natl. Acad. Sci. USA*, 117, 9,  
1076 <https://doi.org/10.1073/pnas.1908670117>, 2020.

1077 104.Stocker, T. F., & Johnsen, S. J.: A minimum thermodynamic model for the bipolar seesaw.  
1078 *Paleoceanography*, 18(4), 1–9. <https://doi.org/10.1029/2003PA000920>, 2003

1079 105.Stouffer, R. J., Yin, J., Gregory, J. M., Dixon, K. W., & Spelman, M. J.: Investigating the Causes of  
1080 the Response of the Thermohaline Circulation to Past and. *Journal of Climate*, 19, 1365–1387.  
1081 <https://doi.org/10.1002/9781119115397.ch25>, 2006

1082 106.Tarasov, L., Dyke, A. S., Neal, R. M., and Peltier, W. R.: A data-calibrated distribution of deglacial  
1083 chronologies for the North American ice complex from glaciological modeling, *Earth Planet. Sci.*  
1084 *Lett.*, 315–316, 30–40, [10.1016/j.epsl.2011.09.010](https://doi.org/10.1016/j.epsl.2011.09.010), 2012

1085 107.Tierney, J. E., Zhu, J., King, J., Malevich, S. B., Hakim, G. J., & Poulsen, C. J.: Glacial cooling and  
1086 climate sensitivity revisited. *Nature*, 584(7822), 569–573. [https://doi.org/10.1038/s41586-020-2617-](https://doi.org/10.1038/s41586-020-2617-x)  
1087 *x*, 2020

1088 108.Timmermann, A., Timm, O., Stott, L., and Menviel, L.: The roles of CO<sub>2</sub> and orbital forcing in  
1089 driving Southern Hemispheric temperature variations during the last 21 000 Yr. *Journal of Climate*,  
1090 22(7), 1626–1640. <https://doi.org/10.1175/2008JCLI2161.1>, 2009

1091 109.Toucanne, S., Zaragosi, S., Bourillet, J.-F., Marieu, V., Cremer, M., Kageyama, M., Van Vliet-Lanoë,  
1092 B., Eynaud, F., Turon, J.-L., and Gibbard, P.-L.: The first estimation of Fleuve Manche palaeoriver  
1093 discharge during the last deglaciation: Evidence for Fennoscandian ice sheet meltwater flow in the  
1094 English Channel ca 20–18 ka ago, *Earth Planet. Sc. Lett.*, 290, 459–473, 2010.

1095 110.WAIS Divide Project Members: Onset of deglacial warming in West Antarctica driven by local  
1096 orbital forcing. *Nature*, 500(7463), 440–444. <https://doi.org/10.1038/nature12376>, 2013.

1097 111.WAIS Divide project members: Precise interpolar phasing of abrupt climate change during the last  
1098 ice age. *Nature*, 520(7549), 661–665. <https://doi.org/10.1038/nature14401>, 2015

1099 112.Weitzel, N., Andres, H., Baudouin, J.-P., Kapsch, M.-L., Mikolajewicz, U., Jonkers, L., Bothe, O.,  
1100 Ziegler, E., Kleinen, T., Paul, A., and Rehfeld, K.: Towards spatio-temporal comparison of simulated  
1101 and reconstructed sea surface temperatures for the last deglaciation, *Clim. Past*, 20, 865–890,  
1102 <https://doi.org/10.5194/cp-20-865-2024>, 2024.

1103 113.Yoshimori, M., Yokohata, T., and Abe-Ouchi, A.: A Comparison of Climate Feedback Strength  
1104 between CO2 Doubling and LGM Experiments, J. Climate, 22, 3374–3395,  
1105 <https://doi.org/10.1175/2009JCLI2801.1>, 2009.

1106 114.Zhu, J. and Poulsen, C. J.: Last Glacial Maximum (LGM) climate forcing and ocean dynamical  
1107 feedback and their implications for estimating climate sensitivity, Clim. Past, 17, 253–267,  
1108 <https://doi.org/10.5194/cp-17-253-2021>, 2021.

1109

1110